Electric Power Systems Research 214 (2023) 108909

Contents lists available at ScienceDirect

Electric Power Systems Research

journal homepage: www.elsevier.com/locate/epsr

Review, analysis, and performance evaluation of the most common four active methods for islanding detection in grid-connected photovoltaic systems

Fadila Barkat [a], Ali Cheknane [a], Josep M. Guerrero [b], Abderezak Lashab [b], Marcel Istrate [c], Mihai Gavrilas [c], Justina G. Motas [c], Ioan Viorel Banu [c,d,*]

[a] LSMF Laboratory, Department of Electronic, Faculty of Technology, Amar Telidji University, Laghouat, 03000, Algeria
[b] The Villum Center for Research on Microgrids (CROM), AAU Energy, Aalborg University, Aalborg East, 9220, Denmark
[c] "Gheorghe Asachi" Technical University of Iasi, Iasi, 700050, Romania
[d] The Department of Power Engineering and Computer Science, Faculty of Engineering, "Vasile Alecsandri" University of Bacau, Bacau, 600115, Romania

ARTICLE INFO

Keywords:
Active frequency drift (AFD)
Active islanding detection method
Photovoltaic system
Sandia frequency shift (SFS)
Slip mode frequency shift (SMS)
Sandia voltage shift (SVS)

ABSTRACT

This paper systematically analyzes the islanding performance under different case studies and scenarios of the most well-known active islanding detection methods (IDMs) for single-phase grid-connected photovoltaic (PV) systems. They are named as follows: Active Frequency Drift (AFD), Sandia Frequency Shift (SFS), Slip Mode frequency Shift (SMS), and Sandia Voltage Shift (SVS) anti-islanding detection strategies. The performance of these four active anti-islanding methods has been examined in detail using Matlab/Simulink. Moreover, the quality factor and non-detection zone (NDZ) influence on islanding detection is also analyzed. According to the new grid codes and standards, the studied active IDMs provide good detection times. Furthermore, the case studies illustrate that these active detection techniques can successfully detect the islanding operation mode under different quality factors, types of loads, solar irradiance changes, and fault-ride through (FRT) operation mode.

1. Introduction

Islanding represents a condition when a section of the electric grid with loads and distributed generation (DG) systems, are separated from the primary power grid and remains to operates [1–4] with local loads [5,6]. Usually, the islanding operation mode is unwanted due to safety issues of the utility grid, or it can lead to asynchronous reconnection [2] that may damage the equipment [7]. Because of these risks, grid codes and standards [8], like IEEE-1547 UL-1741, IEC62116, VDE 0126–1–1, IEEE Std. 929–2000 [4], and IEEE 1547 have been established [9–11]. The dispersed generation and microgrid standards have been recently reviewed in [8]. According to the IEEE 929–2000 [4], to address the issue of islanding, operation detection should be studied by suggesting a methodology for testing the distributed power generation systems (DPGS) [12] as well as protecting the system. Effective and reliable islanding detection methods (IDMs) have been achieved [13–16].

The IDMs can be passive, active, and hybrid [17–20]. The passive islanding methods [6,21] are based on the system parameters measurement [22] such as under/over voltage (UOV) and under/over frequency (UOF) [9,23–25]. The effectiveness of the passive methods depends on the thresholds of the monitored parameters set to identify the islanding operation condition. Usually, the voltage threshold is of 88–110% of the nominal value [10]. The admissible frequency is usually between 59.3 Hz and 60.5 Hz [10,26–28].

The main disadvantage of the passive anti-islanding strategies is that they have a larger non-detection zone (NDZ) [27,29–33]. Many active anti-islanding methods have been elaborated to avoid this drawback [32,34]. The active methods [35,36] generate some perturbations at the point of common coupling (PCC) of the PV system [27,29,37] to change one or more power grid parameters that can be sensed by the passive IDMs [5,22]; thus, minimize the so-called NDZ [29,37,38]. The hybrid methods are new recent techniques, which represent complementary combinations of active and passive methods [39–45]. Artificial intelligence methods [46–48] were proposed for the same purpose [49–51].

* Corresponding author.
E-mail address: ibanu@tuiasi.ro (I.V. Banu).

https://doi.org/10.1016/j.epsr.2022.108909
Received 17 February 2022; Received in revised form 23 May 2022; Accepted 17 October 2022
Available online 27 October 2022

Nomenclature

Abbreviations/Acronyms

AC	Alternating Current
ADF	Active Frequency Drift
DC	Direct Current
DG	Distributed Generation
DPGS	Distributed Power Generation Systems
FDZ	Fault Detection Zone
FRT	Fault-Ride Through
IDM	Islanding Detection Methods
MPPT	Maximum Power Point Tracking
NDZ	Non-Detection Zone
P&O	Perturb and Observe
PCC	Point of Common Coupling
PLL	Phase-Locked Loop
PV	Photovoltaic
PWM	Pulse Width Modulation
RMS	Root Mean Square
ROCOF	Rate of Change of Frequency
SFS	Sandia Frequency Shift
SMS	Slip Mode Frequency Shift
STC	Standard Test Conditions
SVS	Sandia Voltage Shift
THD	Total Harmonic Distortion
UOF	Under/Over Frequency
UOV	Under/Over Voltage
VFP	Voltage-Frequency Protection

Variable/Parameter

C_f	Chopping Factor
C_{f0}	Implicit Chopping Factor
df	AFD Frequency Variation ()
K_{SFS}	SFS Proportional Gain
K_{SVS}	SVS Proportional Gain
P	Active Power
Q	Reactive Power
Q_f	Quality Factor
ΔP	Active Power Variation
ΔQ	Reactive Power Variation
θ_{AFD}	AFD Phase Angle
θ_m	SMS Phase Angle

Table 1
PV system parameters according to IEEE 929–2000 standard.

Parameter		Value
Power of the PV Array [kW]		3.5
Nominal line frequency (f_0) [Hz]		60
Grid voltage (V_g or V_{RMS} LL) [V]		240
DG output power [kW]		3.5
Input DC voltage [V]		434
$f_{(min/max)}$ [Hz]		59.3/60.5
Grid-side inductance filter (L_g) [mH]		2
Inverter-side inductance filter (L_i) [mH]		1.73
Capacitance filter (C_f) [μF]		15
RLC load	Resistance (R) [Ω]	16.457
	Inductance (L) [mH]	17.5
	Capacitance (C) [μF]	404.25
Quality factor (Q_f)		2.5

1.1. Contribution and paper organization

This paper explores the islanding performance of the most used four active IDMs for single-phase grid-connected photovoltaic (PV) systems, as indicated in [34]. Although the unintentional islanding of PV systems has been deeply investigated in the last decade, it is still a timely subject, as new requirements have arisen, such as the performance of these methods under fault-ride through (FRT) required by grid codes. In this study, the Active Frequency Drift (AFD) [52], Sandia Frequency Shift (SFS) [37], Slip Mode Frequency Shift (SMS), and Sandia Voltage Shift (SVS) [53] active islanding methods are studied in detail and considering different cases for load quality factors (Q_f), load types, and irradiance variations. Moreover, the programming code of Matlab Function for the analyzed active methods in Simulink is given. The NDZ of each active method's influence on the quality factor is investigated. Testing the islanding operation of the PV inverter with studied active methods is also analyzed in this paper for different case studies. The results are close to real PV systems using detailed grid-connected PV system modeling in Simulink [54]. Different case studies confirm the validity of the obtained

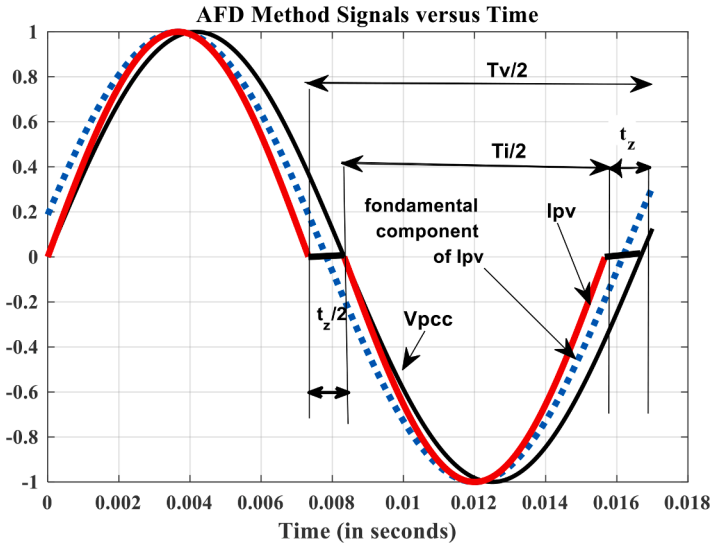

Fig. 1. Simulated waveform used by the AFD method [30,85].

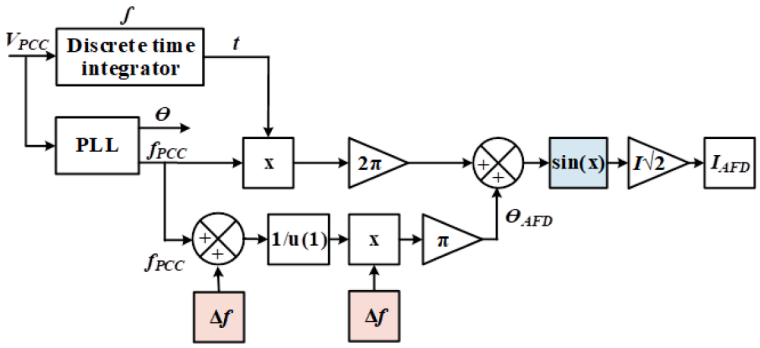

Fig. 2. AFD method block diagram.

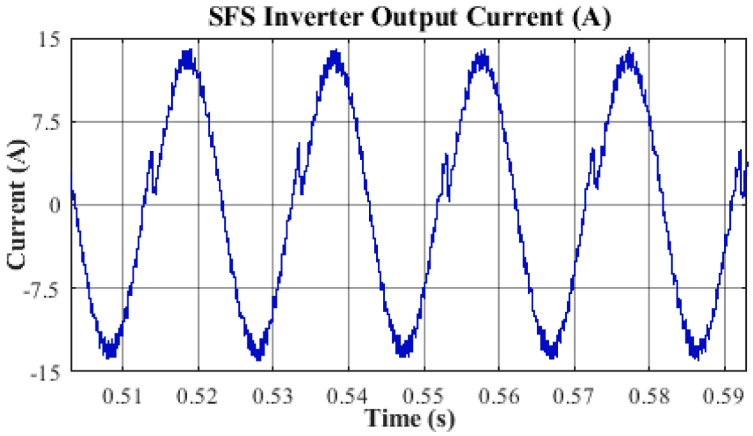

Fig. 3. Simulated inverter current waveform used by the SFS method.

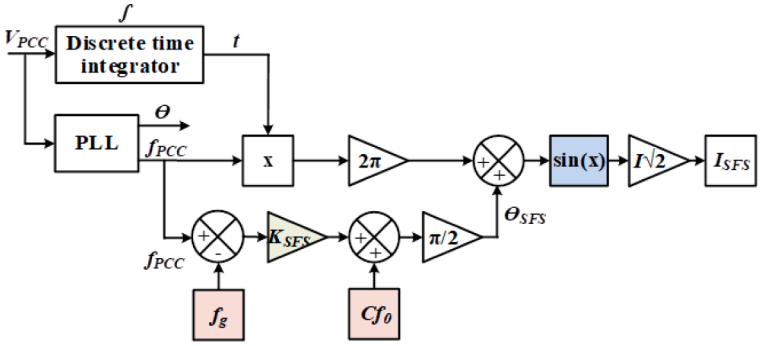

Fig. 4. SFS method block diagram.

simulation results. Some widely used islanding methods like [20,27], and [55] get similar results in the comparison.

This work summarizes of all the most significant methods used in a way in which the studied active methods can be compared and choose the required method under certain conditions by defining their anomalies as their characteristics. The active methods are studied and compared for the first time in this way. The paper's main contribution can be the didactic approach used by the authors so that the researchers can study this subject. Challenging cases of islanding detection, like FRT, have been considered. Under this context, all the files used to simulate the investigated methods are supplied in [56].

The paper's main contribution is analyzing the four most crucial active islanding detection methods for PV systems. The performance of these methods is analyzed in detail and considers different cases for load types, load quality factors, irradiance variations, and fault-ride through an operation. Moreover, the non-detection zone of each method, the influence of the quality factor, and islanding detection times are also studied for different cases. The paper is a reference for other workers and researchers to know which method is appropriate to their systems concerning its limits and results. Each method is studied and tested in different scenarios and complications.

The drawbacks and gaps in the literature are the lack of complete studies with more important IDMs. Only comparative studies with one or two active methods and hybrid methods with one active method and another passive method, like SMS and rate of change of frequency (ROCOF) or SFS and ROCOF hybrid methods, can be found in the literature, but not four important IDMs or hybrid methods with three passive methods. That is a considerable number to compare them well regarding their requirements because they are studied on the same scale. The proposed approach aims at filling these gaps by studying the active methods differently from others' works. This paper studies all analyzed methods in classical and hybridization mode with the three passive

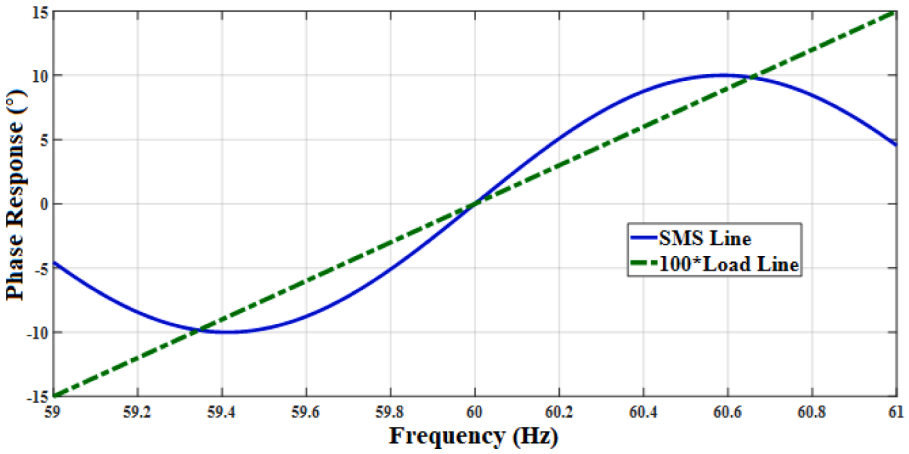

Fig. 5. Local load and SMS line as a function of frequency.

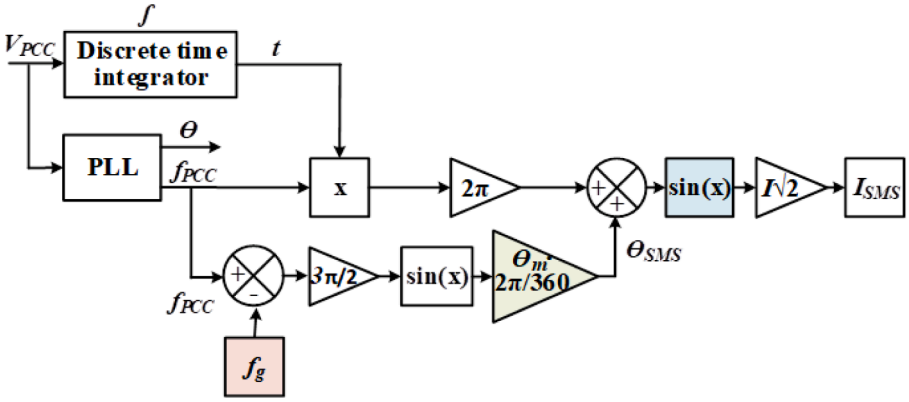

Fig. 6. SMS method block diagram.

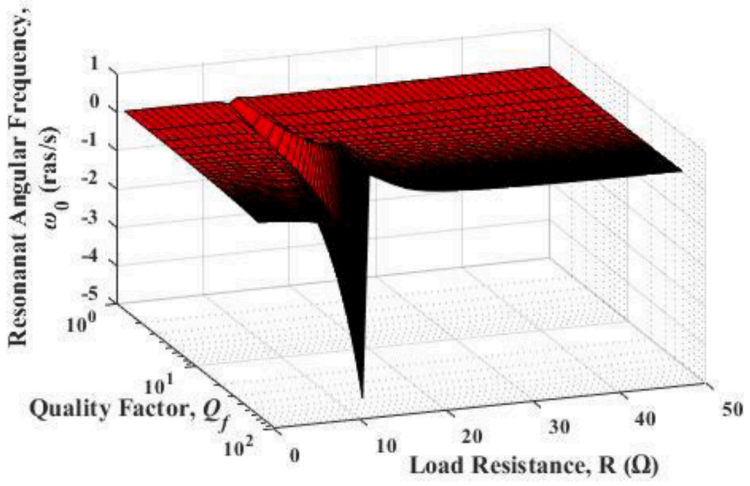

Fig. 7. NDZ of SVS method.

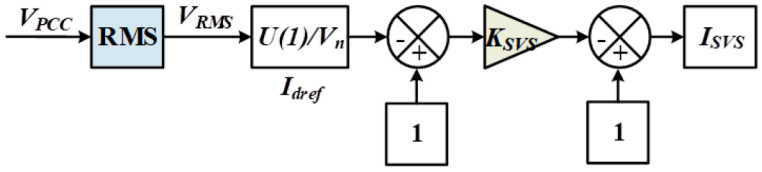

Fig. 8. SVS method block diagram.

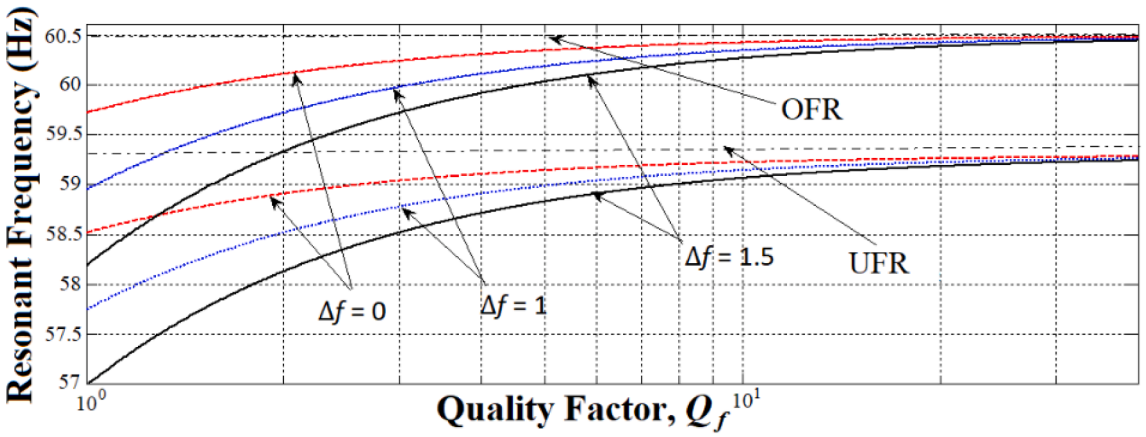

(a)

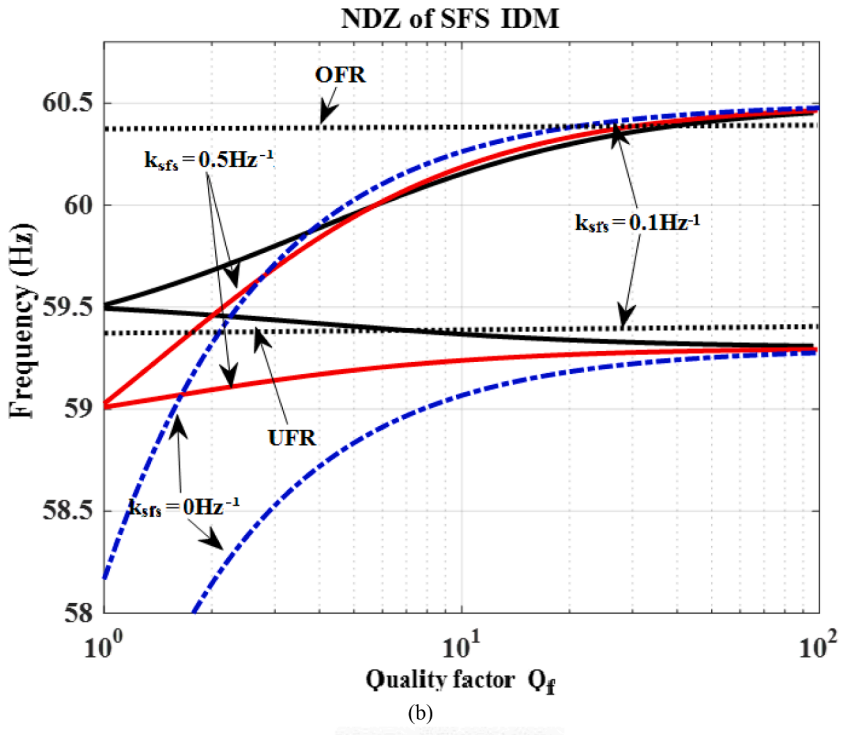

(b)

Fig. 9. (a) NDZ of AFD method. (b) NDZ of the SFS method. (c) NDZ of SVS method. (d) NDZ of SMS method.

methods to cover most possibilities to develop novel IDMs.

The paper is organized as follows. Section 2 presents a systematic analysis of four active anti-islanding methods, which are namely the AFD, SFS, SMS, and SVS active detection algorithms, with their mathematical modeling using the NDZ and quality factor. The influence of the quality factor on these active islanding methods is evaluated in the same section. The developed single-phase grid-tied PV system and its testing with analyzed active IDMs considering the standard operating conditions of each anti-islanding detection algorithm are shown in Section 3. Section 4 presents the results of the studied active IDMs considering different load quality factors, types of loads, and irradiation effect conditions on each active method, as well as the evaluation of effectiveness of the active islanding methods in hybrid detection strategies with passive islanding prevention methods. In the last section, the main conclusions of this research are presented.

2. Description of the PV system under anti-islanding test

To avoid inherent mismatches between the results from software based simulations and hardware or real-time simulations, the implemented PV system [54] and all studied IDMs [34] are independently validated in Simulink.

2.1. Studied grid-connected PV system

The testing PV system relates to the one in [54]. The schematic of the developed PV system is given in Fig. 12 [34]. It is composed of: a 3.5 kW peak power PV solar array of one string with 14 PV modules Trina Solar TSM-250PA05.08 [54], a full-bridge IGBT inverter, an inverter control system, an MPPT controller with perturb and observe (P&O) method [54,95] a block that measures the PCC voltage, current, frequency, an IDMs block which injects currents in the power grid [54], a disconnecting block based on the ROCOF [3,9] and voltage-frequency

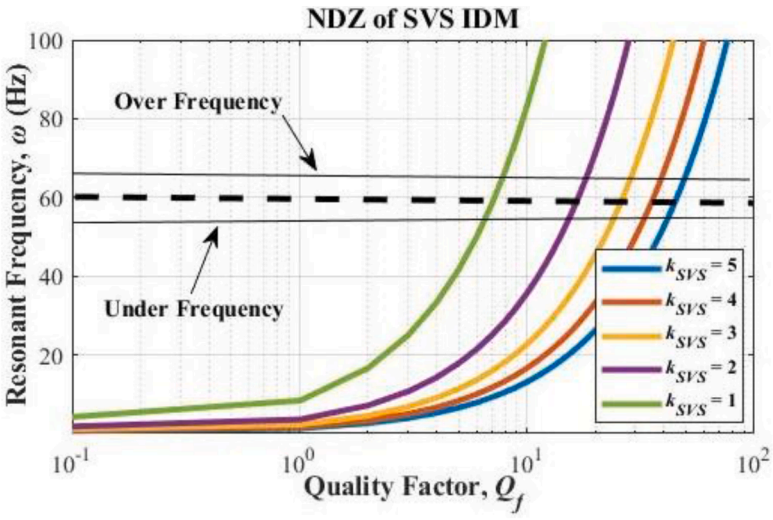

(c)

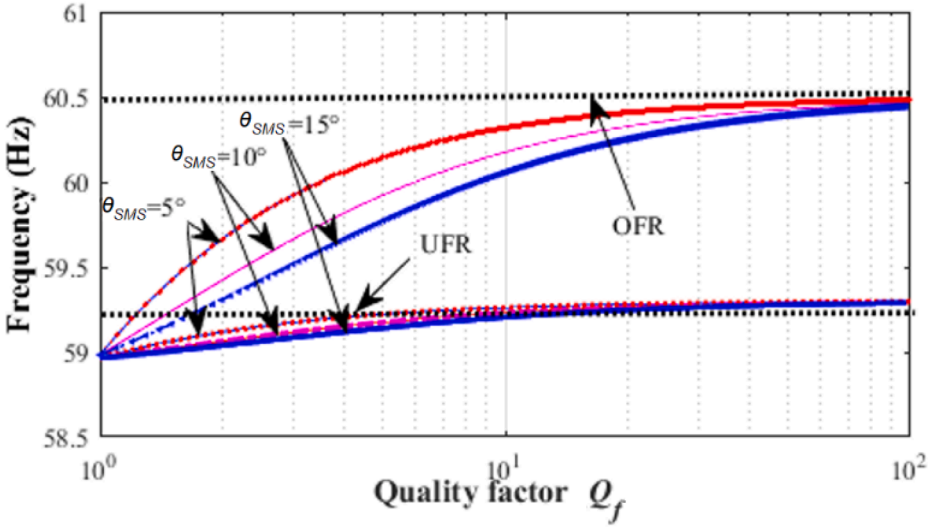

(d)

Fig. 9. (*continued*).

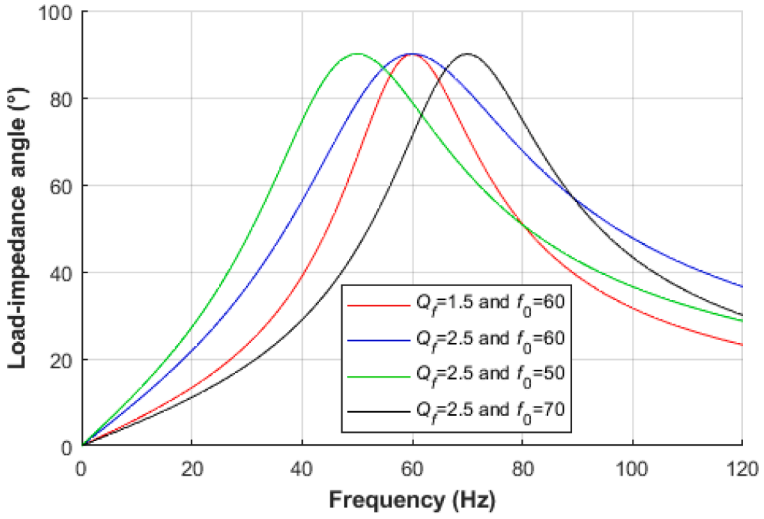

Fig. 10. Load-impedance phase angle as function of the frequency [27,85].

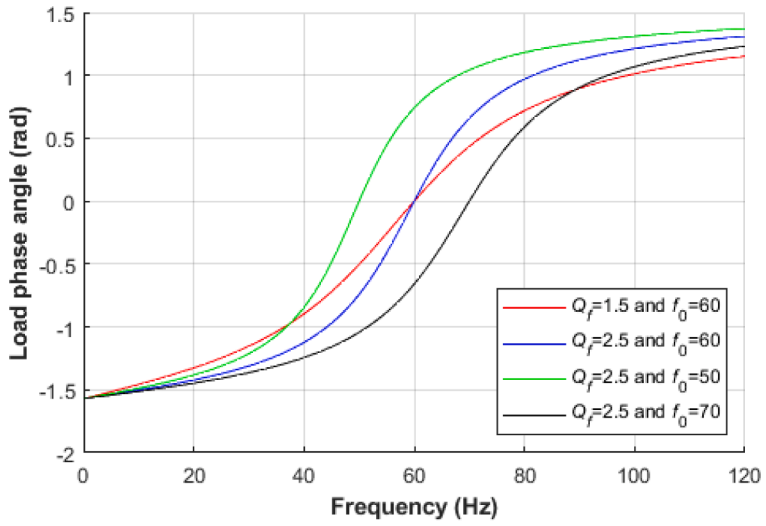

Fig. 11. Load phase angle function on frequency [13,85].

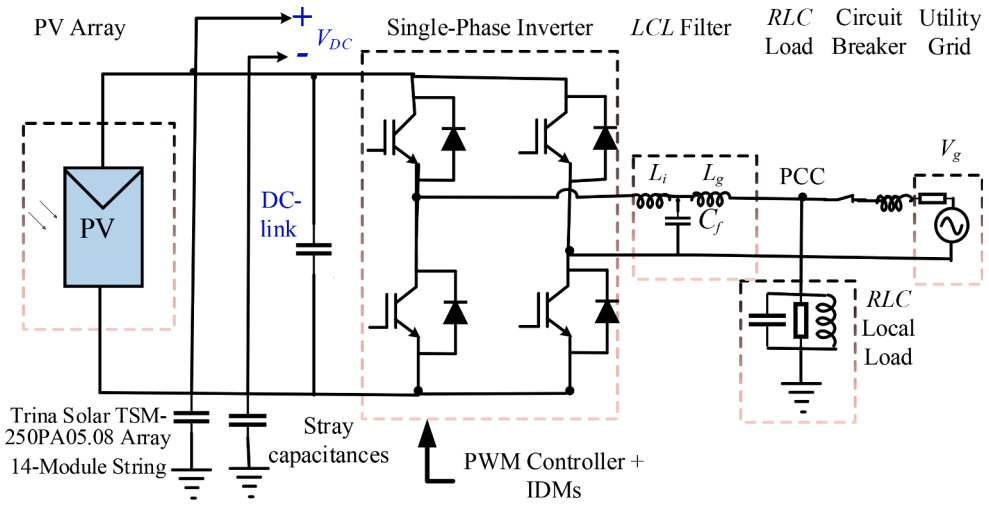

Fig. 12. Testing PV system model.

Table 2
Simulation results of analyzed active methods.

Active methods	Parameters	Detection Time (ms)	
		VFP	ROCOF
AFD	$df = 1.5$ Hz	132.0	519.2
	$df = 1$ Hz	182.2	202.1
	$df = 0.5$ Hz	323.19	219.0
SFS	$K_{SFS} = 0$ Hz^{-1}	130.7	119.9
	$K_{SFS} = 0.018$ Hz^{-1}	148.4	119.5
	$K_{SFS} = 0.05$ Hz^{-1}	148.1	133.5
SMS	$\theta_m = 25°$	231.2	223.9
	$\theta_m = 15°$	285.8	221.4
	$\theta_m = 10°$	783.0	220.8
SVS	$K_{SVS} = 1$ A/V	428.0	120.1
	$K_{SVS} = 0.5$ A/V	615.0	120.7
	$K_{SVS} = 0.1$ A/V	841.0	220.0

protection (VFP) [96] passive methods. When the breaker is opened, an islanding operation mode is activated [96].

A PWM-controlled single-phase power inverter [54,82] with an *LCL* filter is used in this research. An inverter control system with a P&O-based MPPT controller [97,98], DC voltage and current regulators, phase-locked loop (PLL) [99–101], measurements [9], and a PWM generator are used to control the PV power inverter [54]. The MPPT controller [102] collects the maximum electric power from the PV solar array under varying weather conditions [103].

The used PV inverter transforms the 434 V DC link voltage of a 3.5 kW PV solar array at 1000 W/m^2 and 25 °C, which are the standard test conditions (STC), to the utility grid voltage, which is 240 V AC at 60 Hz frequency [54]. Finally, a 240 V–14.4 kV low frequency transformer was connected to the PV inverter [104]. The principal-built simulation model parameters are listed in Table 1.

The anti-islanding method works on the principle of UOV and UOF prevention, after which the islanding operation mode is detected. The islanding mode appears in all analyzed scenarios at the circuit breaker opening at $t = 0.5$ s [34]. The active methods are carried out on a PV-based DG unit which consists of a PV solar array, a PV inverter that is operating using P&O based MPPT controller as in [54,103], and [105], and an *LCL* filter, and a switch (circuit breaker or fuse). Moreover, a utility grid with a 240 V transformer, an ideal AC source of 14.4 kV RMS, and a parallel *RLC* load from [54] which has parameters to do the $Q_f = 2.5$ as in [13] and [84], are adapted.

2.2. Studied active islanding detection methods

The studied active IDMs are detailed in this section. The active

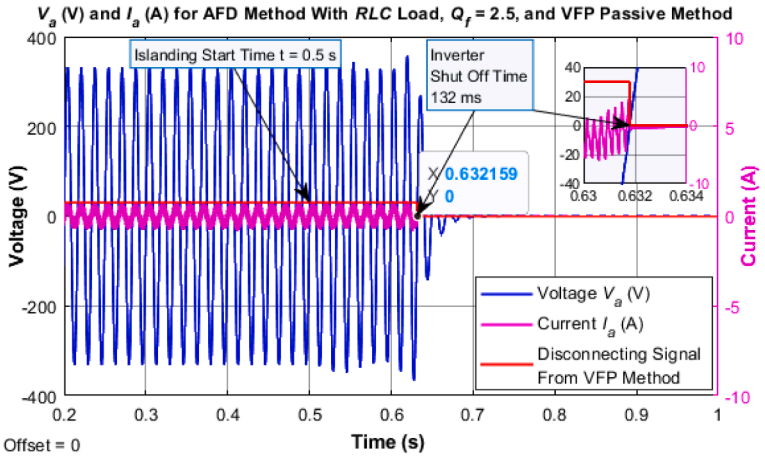

Fig. 13. PV inverter response under islanding operation with AFD method and df =1.5 Hz: PCC voltage, PCC current, and disconnecting signal waveform.

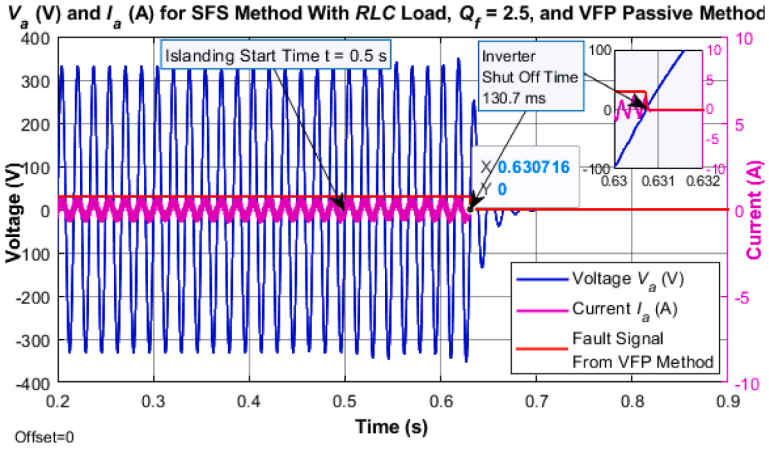

Fig. 14. PV inverter response under islanding with SFS method and $K_{SFS} = 0$ Hz^{-1}: PCC voltage, PCC current, and disconnecting signal.

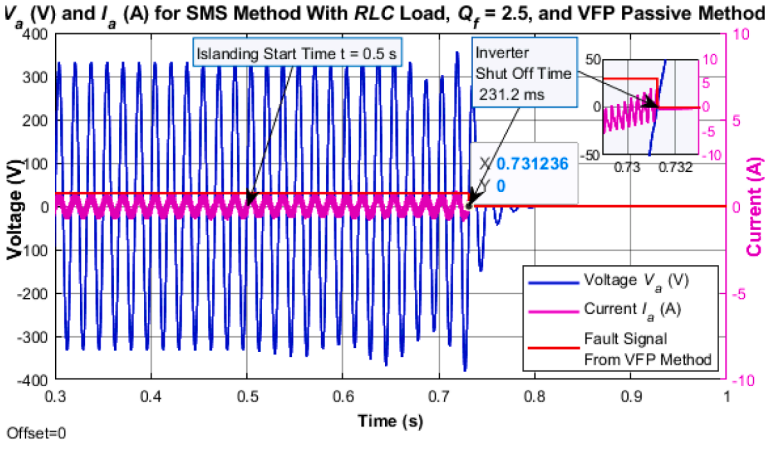

Fig. 15. PV inverter response under islanding with SMS method and $\theta_m = 25°$: PCC voltage, PCC current, and disconnecting signal.

islanding methods are detailed as they are presented in the literature. Furthermore, the developed Matlab models, including the corresponding Matlab Function codes, are presented, where the NDZ is examined and discussed in detail to evaluate these methods. Finally, the General Electric (GE) schemes are given in [57].

Although there are many good quality islanding detection papers, the active IDMs are not studied profoundly. Several papers about active islanding protection (detection) were analyzed, such as [58–80]. Next, some widely used active methods are introduced in the comparison.

2.2.1. *Active frequency drift method*

The AFD technique influences the output current waveform of the PV solar power inverter [30,32], as illustrated in Fig. 1 [81]. During the first segment of the first semi-cycle, the output inverter current is sinusoidal with slightly higher frequency than the rated inverter current [30]. Δf is the difference between the output current frequency and the nominal

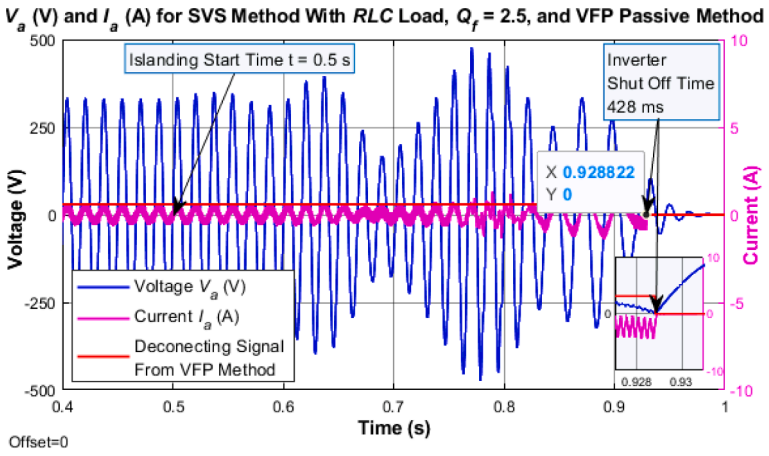

Fig. 16. Inverter response under islanding with SVS method and $K_{SVS} = 1$ A/V: PCC voltage, PCC current, and fault disconnecting signal.

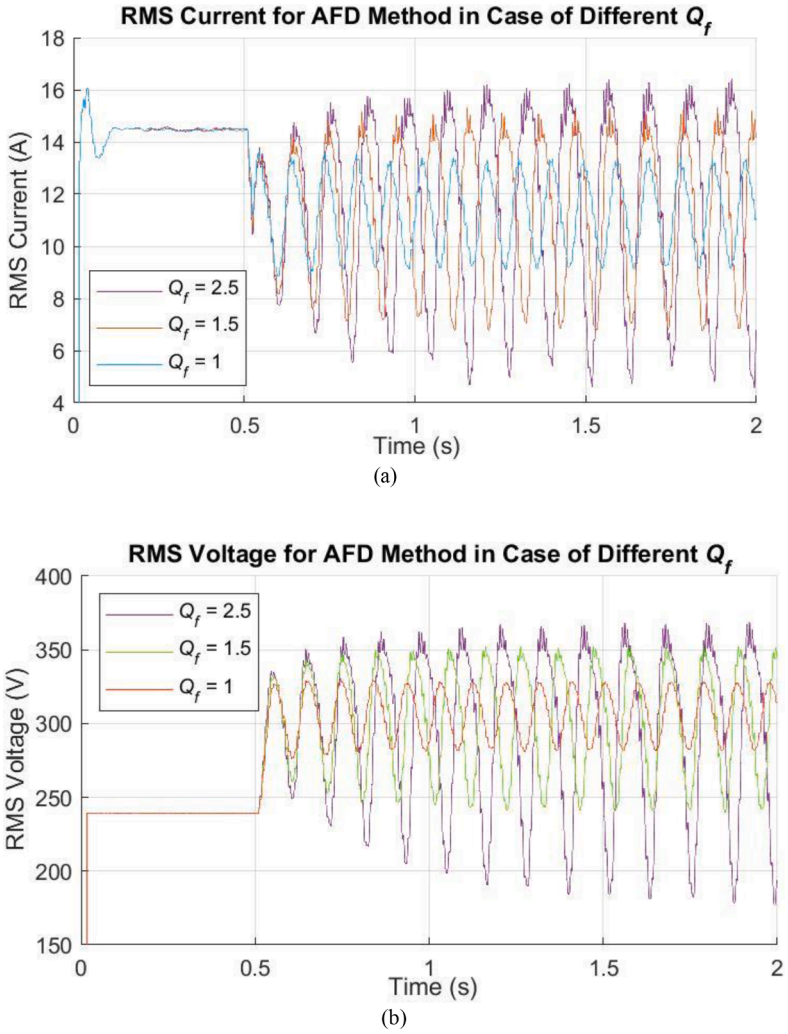

Fig. 17. Results of AFD anti-islanding method under different quality factors. (a) RMS grid current. (b) RMS grid voltage. (c) Reactive power. (d) Active power.

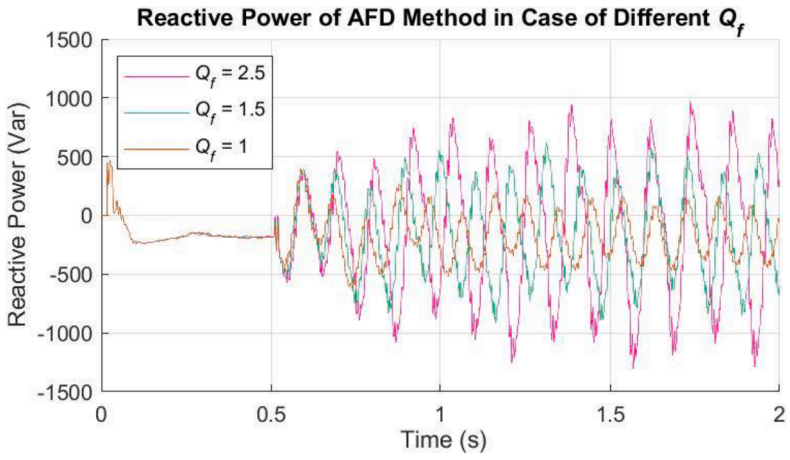

(c)

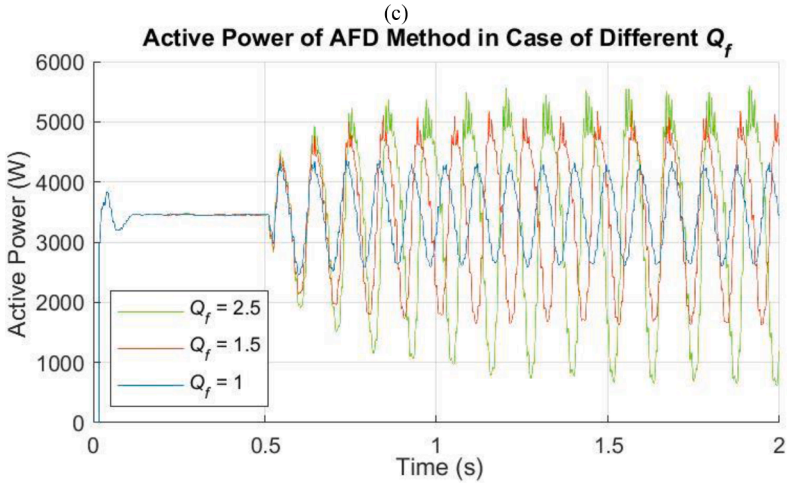

(d)

Fig. 17. (*continued*).

grid frequency [30]. Once the current becomes null, it remains null for a dead time (t_z) until the positive semi-cycle of the signal starts [30,32]. During the last segment of the second semi-cycle, once the current becomes null, it remains null until another cycle starts [30,32].

The inverter current of the AFD technique during each cycle is given by (1) [13,82]:

$$I_{AFD} = \sqrt{2}I\sin[2\pi ft + \theta_{AFD}] \quad (1)$$

where I represents the phase peak current [83], f represents the utility grid frequency in the PCC [84], t represents the time, and θ_{AFD} represents the angle of the AFD active technique [34]. For example, under islanding operation mode, the AFD phase angle θ_{AFD} can be expressed as follows [13,82]:

$$\theta_{AFD} = \pi \cdot \frac{\Delta f}{\Delta f + f} \quad (1)$$

where, $\Delta f = f - f_g$ and f_g is the nominal grid frequency (60 Hz).

The power grid maintains the frequency of the grid-connected PV system. However, when the power grid is disconnected, the current injected by the inverter gives the PCC frequency. Therefore, it drifts far away from the rated grid frequency until the UOF protection relay identifies the islanding mode [30]. Fig. 2 represents the AFD block diagram. The developed Simulink block for the AFD method with Matlab Function block comprises the following code:

```
function y = fcn(f,id,iq)
  %#codegen
  % ***********
  %% AFD Method
  % ***********
  df=1.5;
  x=(pi*df)/(f+df);
  a=cos(x);
  b=-sin(x);
  c=sin(x);
  d=cos(x);
  y=zeros(2,1);
  y(1,1)=(a.*id)+(b.*iq);
  y(2,1)=(c.*id)+(d.*iq);
```

2.2.2. Sandia frequency shift method

The SFS active islanding detection technique enhances the AFD islanding performance by a positive feedback [30,86] to drift faster the grid frequency far away from the rated grid frequency [30,32]. Therefore, the SFS method has a significantly smaller NDZ than the AFD method [30].

The SFS inverter current is given by (3) [13,30]:

$$I_{SFS} = \sqrt{2}I\sin[2\pi ft + \theta_{SFS}] \quad (2)$$

where θ_{SFS} is the SMS phase angle. The chopping factor (C_f) is modified

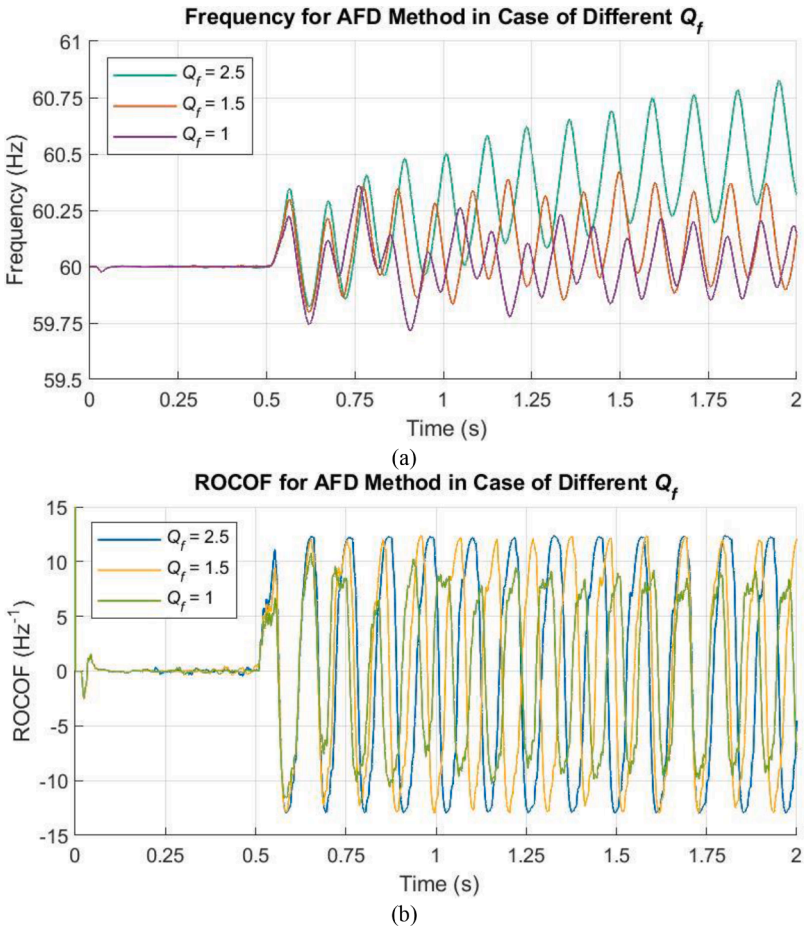

Fig. 18. AFD islanding method under different quality factors. (a) Frequency. (b) ROCOF.

depending on the measured frequency drift as below [13,30]:

$$C_f = C_{f_0} + k(f - f_g) \tag{4}$$

where k is a positive feedback gain and C_{f0} is the implicit chopping factor [30]. Then, the SFS phase angle can be written as [13]:

$$\theta_{SFS} = \frac{cf_0 + k(f - f_g)}{2} \tag{5}$$

The SFS current is given in Fig. 3 [86]. Accordingly, the SFS active method block diagram would be as depicted by Fig. 4. The Matlab Function code for the SFS active method is:

```
function y = fcn(f,id,iq)
  %#codegen
  % ***********
  %% SFS Method
  % ***********
  cf=0.04;
  ksfs=0.1;
  x=(pi/2)*(cf+ksfs*(f-60));
  a=cos(x);
  b=-sin(x);
  c=sin(x);
  d=cos(x);
  y=zeros(2,1);
  y(1,1)=(a.*id)+(b.*iq);
  y(2,1)=(c.*id)+(d.*iq);
```

2.2.3. Slip mode frequency shift method

The SMS technique modifies the inverter current phase angle [30,84,86] according to the measured frequency [87] variation and compares it with the rated grid frequency [30,32]. Here, the SMS phase angle is given by (6) [13]:

$$\theta_{sms} = \frac{2\pi}{360}\theta_m \sin\left(\frac{\pi}{2}\frac{f - f_0}{f_m - f_0}\right) \tag{6}$$

where f_0 represents the resonant frequency of the *RLC* load and f_m represents the frequency when θ_m arises. f_m-f_0 = 3 Hz [30,88]. Consequently, the SMS current can be expressed as follows [13]:

$$I_{SMS} = \sqrt{2} I \sin[2\pi f t + \theta_{SMS}] \tag{7}$$

Fig. 5 reveals the SMS frequency curve from 59.3 Hz to 60.5 Hz. The SMS phase angle θ_{sms} in (6) is assumed to be sinusoidal, while the load line appears illustrated as a parallel *RLC* load with a positive ramp [13]. Regardless of the connected load, the grid frequency determines the grid-connected inverter's current phase angle [89]. When the islanding mode occurs, the frequency varies around zero [89], situated at the intersection of the SMS and load lines, as depicted in Fig. 5. Here, the islanding mode occurs when [13]:

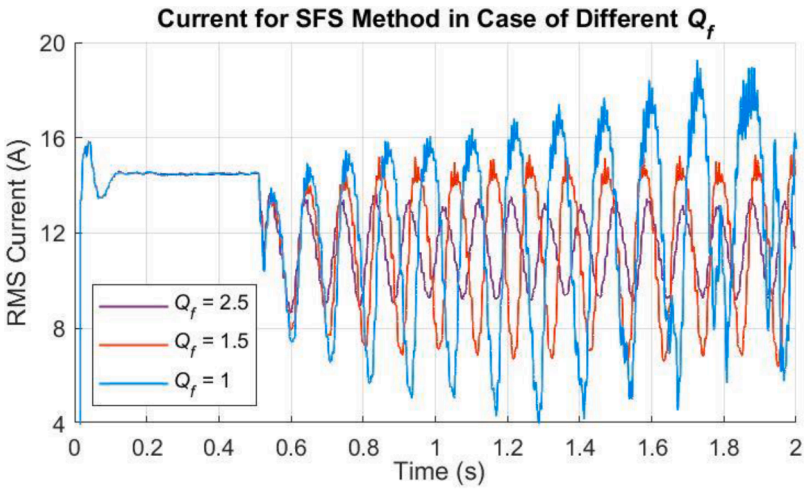

Fig. 19. SFS method for different Q_f. (a) RMS grid current. (b) RMS grid voltage. (c) Reactive power. (d) Active power.

$$\frac{d\theta_{load}}{df}|_{f=f_g} \leq \frac{d\theta_{sms}}{df}|_{f=f_g} \tag{8}$$

Using the same reasoning and procedure reported in [37,84], it can be stated that the islanding mode in term of the phase angle can be obtained like the following [85]:

$$\theta_m \geq \frac{12Q_f}{\pi^2}\left(f_m - f_g\right) \tag{9}$$

When the grid frequency is slightly raised after disconnecting the grid, the current phase angle increases while the time of the next zero-crossing PCC voltage decreases. The PV inverter control detects, recognizes, and identifies this as the frequency increases again. Therefore, the inverter's current phase angle increases until the frequency exceeds the limit. When the electrical network is disconnected, the PCC frequency decreases continuously until being identified by the under-frequency protection relay [30,89].

The SMS method block diagram would be as shown in Fig. 6. The coding for the Matlab Function of the developed Simulink block of the SMS method is related as follows:

```
function y = fcn(f,id,iq)
  %#codegen
  % **********
  %% SMS Method
  % ***********
  cf=0.04;
  ksms=0.08;
  x=(pi/2)*(cf+ksms*(f-60));
  a=cos(x);
  b=-sin(x);
  c=sin(x);
  d=cos(x);
  y=zeros(2,1);
  y(1,1)=(a.*id)+(b.*iq);
  y(2,1)=(c.*id)+(d.*iq);
```

2.2.4. *Sandia voltage shift method*

The SVS technique [9,35] utilizes a positive feedback [86] on the PCC voltage [32] like the active power strategy. When the PCC voltage

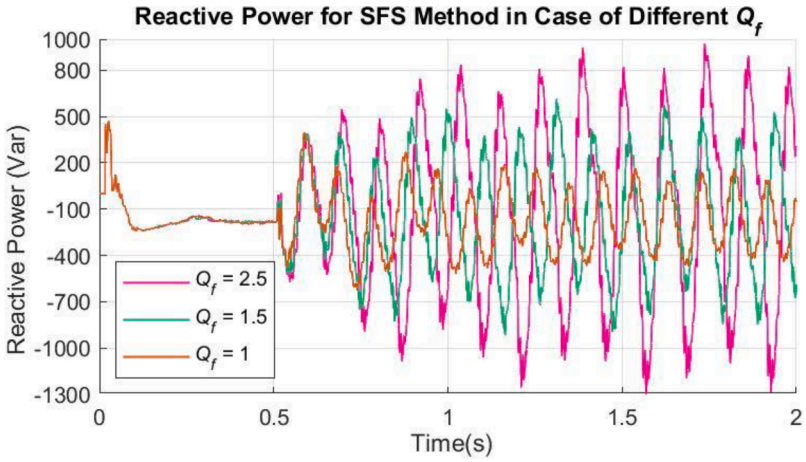

(c)

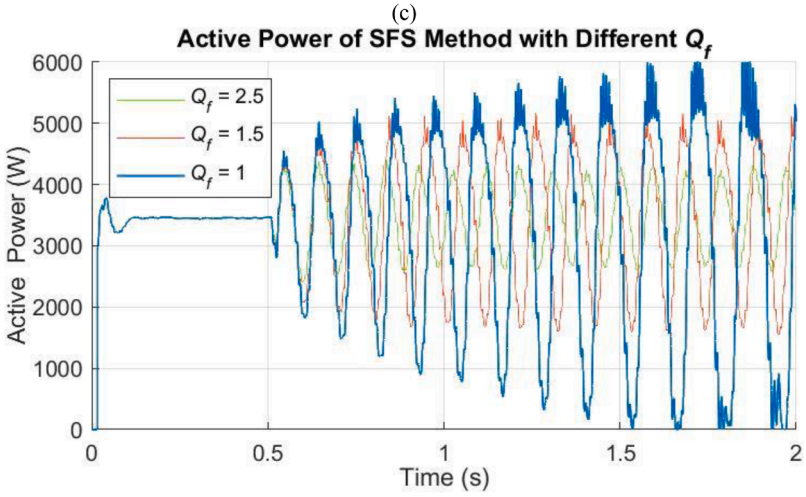

(d)

Fig. 19. (*continued*).

decreases, the output PV inverter current decreases, and the power yield from the PV system. The reaction time can be balanced by the factor k_v, which decreases or increases the PV inverter current relative to the voltage change. Consequently, the same principle used in the active power control can be considered here. Finally, this active technique derives the voltage adequacy past the UOV limits, permitting the islanding detection. Lowering the disturbance voltage is preferable rather than expanding it to keep away from any potential harm to the associated hardware.

The SVS technique is an accessible and highly compelling approach among the positive feedback techniques. Moreover, the SVS and SFS active anti-islanding techniques enhance the phenomenon adequacy at execution. However, the SVS active technique has two disadvantages. First, the grid voltage is constantly perturbed, which disturbs the power quality, and second, the efficiency/performance of the Maximum Power Point Tracking (MPPT) controller can also be influenced [9,35].

The PV inverter current reference can be computed from the following relationship [9,35]:

$$I_{ref} = \frac{k_v \cdot \Delta V + P_{DG}}{V} \tag{10}$$

where $\Delta V = V\text{-}V_{nom}$ represents the voltage change, V represents the deliberately imposed voltage at the PCC point, and V_{nom} represents the nominal voltage [86].

In Fig. 7, the NDZ of the SVS algorithm is depicted. The SVS method block diagram would be as depicted by Fig. 8. The programming code of Matlab Function for SVS method is:

```
function y = fcn(v,id)
  %#codegen
  % ***********
  %% SVS Method
  % ***********
  ksvs=1;
  y=id+ksvs*(v-240)/240;
```

2.3. Non-detection zone of studied active methods

To establish the NDZ of the studied active islanding methods, the phase angle between the voltage and current must be approximated. Consequently, the phase angles of the adapted active techniques are analyzed to evaluate these active detection methods [84,90].

Usually, the reactive power balance condition is defined using the loads and inverter's currents phase angles φ_{load} and φ_{inv}, respectively [84,90]. Therefore, the steady-state frequency value of a PV inverter in islanding operation mode is determined using the phase criterion as follows [84,90]:

$$\varphi_{inv} = \varphi_{load} \tag{11}$$

Here, drift frequency techniques are efficient when (12) [84]:

$$\varphi_{inv} > \varphi_{load} \tag{12}$$

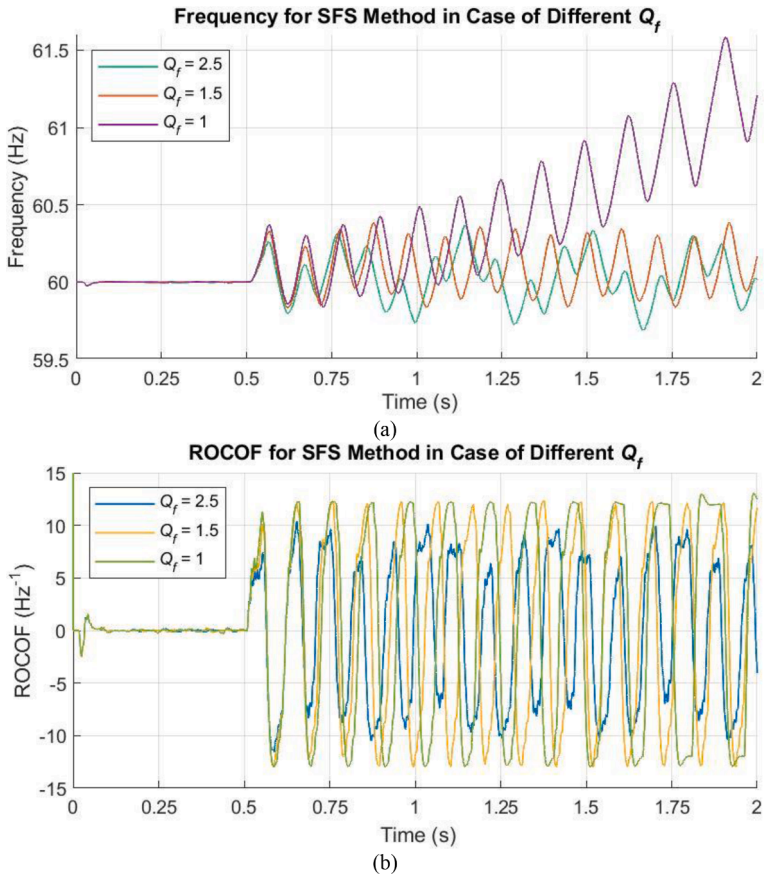

Fig. 20. SFS method for different Q_f. (a) Frequency. (b) ROCOF.

The parallel *RLC* load phase angle φ_{load} can be determined as follows [84,90]:

$$\varphi_{load} = tan^{-1}\left[Q_f\left(\frac{f_0}{f}-\frac{f}{f_0}\right)\right] \tag{13}$$

The PV inverter phase angle φ_{inv} in the case of AFD method can be calculated as [13,84,91]:

$$\varphi_{inv\_AFD} = \pi.\frac{\Delta f}{f+\Delta f} \tag{14}$$

In a similar way, for the SFS [92] and SMS techniques [84]:

$$\varphi_{inv\_SFS} = \frac{\pi}{2}\left[cf_0 + k\left(f - f_g\right)\right] \tag{15}$$

$$\varphi_{inv\_SMS} = \theta_m \sin\left(\frac{\pi}{2}\frac{f-f_g}{f_m-f_g}\right) \tag{16}$$

The NDZ for each IDM is achieved by estimating the frequency concerning the quality factor Q_f [84]. The simulation tests consider the standard operating conditions of the previously detailed methods. The frequency variations of AFD method have been analyzed using different values of Δf (0.5 Hz, 1 Hz, and 1.5 Hz). The SFS technique was analyzed for three cases of accelerating the frequency gain K_{SFS} (0 Hz^{-1},0.018 Hz^{-1}, and 0.05 Hz^{-1}) [49]. For the SMS technique, three values of θ_m were analyzed (5°, 10°, and 15°). According to the IEEE Std. 929–2000 [4], the grid's circuit breaker opens after six cycles at the beginning to ensure the island mode. Thus, the grid's circuit breaker is disconnected at $t = 0.5$ s. The I_{PCC} grid current is given by (17) [13]:

$$I_{PCC} = \frac{\sqrt{2}}{R}V_g \tag{17}$$

The derived relation between the voltage/frequency and power mismatch thresholds is expressed by (18) and (19) [29,89]:

$$\left(\frac{V_{pcc}^2}{V_{min}}\right)^2 - 1 \le \frac{\Delta P}{P} \le \left(\frac{V_{pcc}^2}{V_{max}}\right)^2 \tag{18}$$

$$Q_f \cdot \left(1 - \left(\frac{f_{PCC}^2}{f_{min}}\right)^2\right) \le \frac{\Delta Q}{P} \le Q_f \cdot \left(1 - \left(\frac{f_{PCC}^2}{f_{max}}\right)^2\right) \tag{19}$$

where, V_{max}, V_{min}, and f_{min}, f_{max} are the UOV and UOF boundaries. In compliance with IEEE 929–2000 Standard [4], the NDZ boundaries [4] for the UOV, UOF, and Q_f have been specified as 0.88 p.u. to 1.1 p.u., 59.3 Hz to 60.5 Hz, and 2.5, respectively [29,34]. Therefore, will be obtain [29]:

$$-17.36\% \le \Delta P/P \le 29.13\% \tag{20}$$

$$-5.94\% \le \Delta Q/P \le 4.11\% \tag{21}$$

When ΔP and ΔQ balance is small beside active power P or reactive power Q [30,34,93], the voltage and frequency variation will not be sufficient to activate the UOV/UOF protections. Therefore, the islanding operation mode cannot be detected [30]. Subsequently, the detecting probability of the islanding operation mode with these active techniques is high [30]. Therefore, at this moment, the AFD, SMS, SFS, and SVS methods were utilized to drift the voltage and frequency outside the limits with a smaller power mismatch [29,93].

The NDZ of the studied AFD, SFS, SMS [13], and SVS active anti-islanding methods appear in Fig. 9. The PV inverter steady-state frequency in the islanding operation mode will be outside the voltage/frequency protection relays limits [37]. The PV inverter will then be tripped [37]. The intersections between the UOV/UOF lines and the

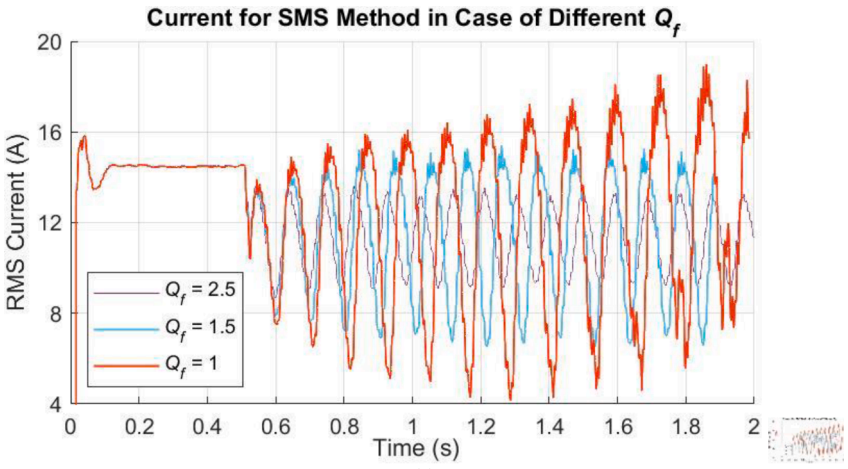

(a)

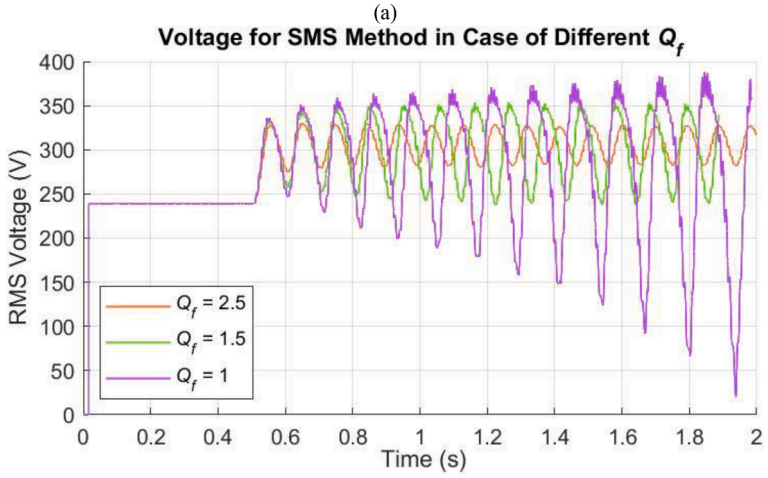

(b)

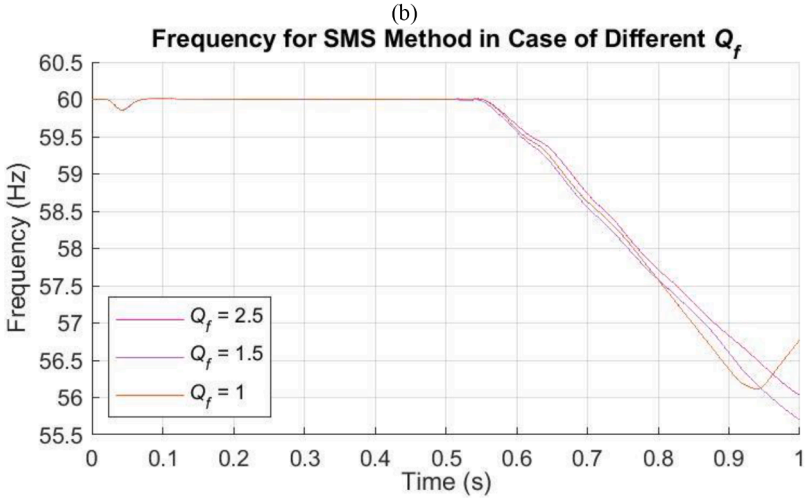

(c)

Fig. 21. SMS method for different quality factors. (a) Current. (b) Voltage. (c) Frequency.

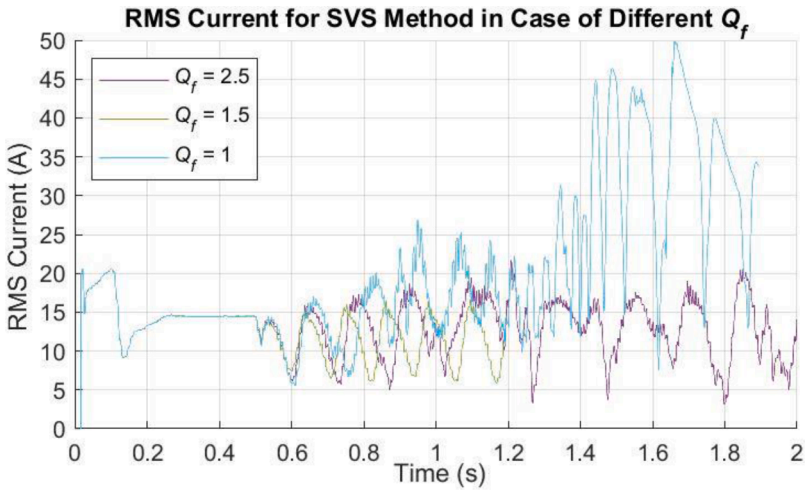

(a)

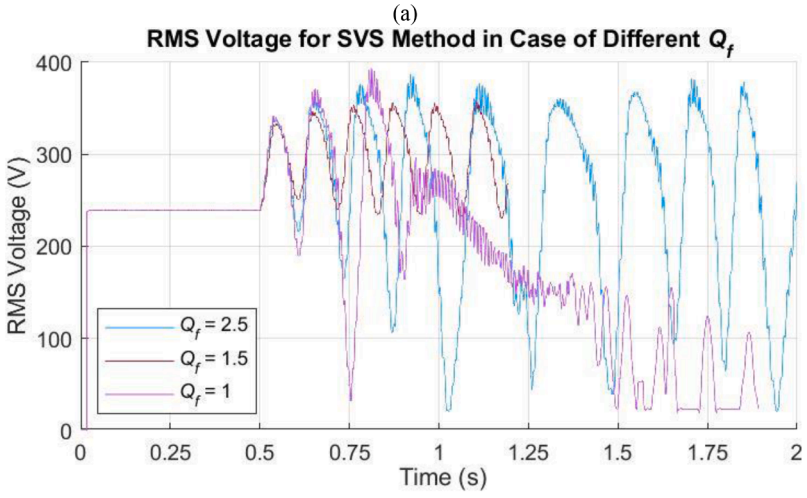

(b)

Fig. 22. Obtained results for SVS method at different Q_f. (a) RMS grid current. (b) RMS grid voltage. (c) Reactive Power. (d) Active power.

achieved curves form the NDZ of each active anti-islanding technique.

2.4. Quality factor influence on islanding operation

The quality factor of a parallel *RLC* load represents the ratio between the stored and dissipated energies per period at a specific frequency [4, 13] and is expressed as follows [13,85,91]:

$$Q_f = \frac{2\pi\left(\frac{1}{2}CR^2I^2\right)}{\frac{\pi RI^2}{w_0}} = w_0RC = \frac{R}{w_0L} = R\sqrt{\frac{C}{L}} \tag{22}$$

where $w_0 = (1/LC)$ is the load resonant frequency pulsation. The parallel *RLC* load impedance phase and magnitude concerning the f arbitrary and f_0 resonant frequencies are expressed as in (23) and (24) [13,85,91]:

$$\varnothing_{load} = \tan^{-1}\left[R\left(\frac{1-\omega^2LC}{\omega L}\right)\right] = \tan^{-1}\left(Q_f\frac{f_0}{f} - \frac{f}{f_0}\right) \tag{23}$$

$$z = \frac{1}{\frac{1}{R} + \left(\frac{1}{\omega L} - \omega C\right)^2} = \frac{R}{\sqrt{1 + Q_f^2\left(\frac{f_0}{f} - \frac{f}{f_0}\right)^2}} \tag{24}$$

The power mismatch space dP versus dQ cannot establish the NDZ of active techniques since, for a determined reactive power mismatch, there might be more combinations of inductance L and capacitance C, [13,89,94]. However, using the load quality factor Q_f as a parameter, different *RLC* load combinations can be governed [85].

The islanding frequency and voltage magnitude at steady-state, V_{island} and f_{island}, respectively, in the case of a *RLC* circuit, are given as the following [13,85]:

$$P_{load,island} = \frac{V_{island}^2}{R} = P_{inv} \tag{25}$$

$$Q_{load,island} = \left(\frac{V_{island}^2}{X_{c,grid}}\left(\frac{f_0^{\,2}}{f_{island}}\right)^2 - 1\right) = Q_{inv} \tag{26}$$

Therefore, it can be stated that the voltage in an islanding operation mode V_{island} is influenced by the active inverter power P_{inv} and resistance R [85]. Next, the frequency f_{island} is drifted by changing the inverter reactive power Q_{inv}. Here, a slight change in the reactive inverter power is necessary to drift φ_{load} frequency outside the specified boundaries [13]. In the case of a *RLC* load, the phase angle of loads versus frequency curves for different resonant frequencies f_0 and Q_f are depicted in Fig. 10. The variation of load phase angle with the frequency with different resonant frequencies f_0 and different quality factors Q_f would be as depicted in Fig. 11 [13,85].

2.5. Testing of studied active islanding detection methods

This section shows the testing system development with analyzed active methods. Simulation of the PV system with all studied methods was performed as in the literature using the PV system model developed

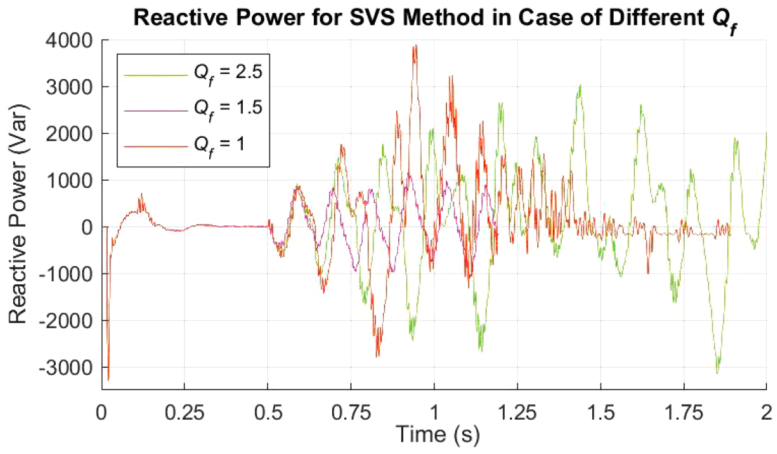

(c)

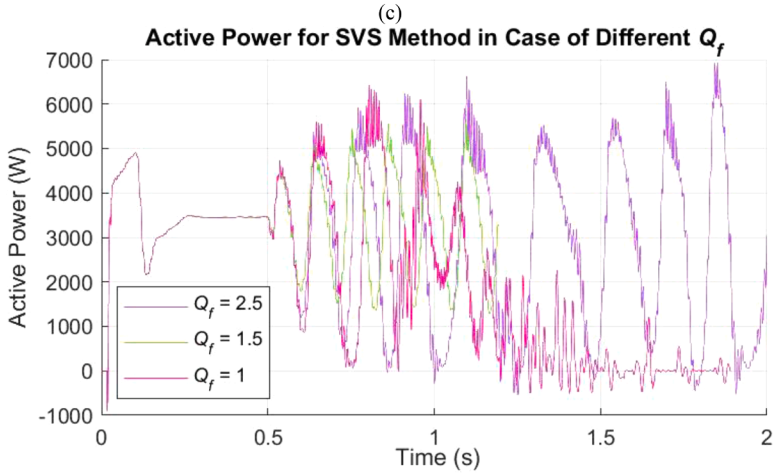

(d)

Fig. 22. (*continued*).

under the Matlab/Simulink. Table 2 illustrates the obtained simulation results.

Each method has used the recommended parameters in the scientific literature within 2 s time as demanded by the IEEE 929–2000 [4] and IEEE 1547.1 [106] standards, as stated in Section 2.3. According to the IEEE Std. 929–2000 [4], the test load represents a resonant parallel *RLC* load [30]. Therefore, the f_0 simulation step has been set to 0.1 Hz. Table 1 indicates the load parameters. The inverter injects the active power from the PV solar array into the grid while the reactive power is nulled. The PV inverter control has a significant role in the case of active IDMs; therefore, more case scenarios will be detailed in Section 3.

Following the testing simulation results, the AFD active method with $\Delta f = 0.5$ Hz and VFP passive method detect the islanding operation mode slower. In contrast, the AFD active method with $\Delta f = 1.5$ Hz detects islanding operation faster than the case when the system with $\Delta f =$ 1 Hz (see Table 2). Given this, Fig. 13 depicts the studied PV power system response with the AFD method and VFP relay in terms of the V_{PCC}, I_{PCC} phase current, and disconnecting signal, considering only the $\Delta f = 1.5$ Hz case.

Fig. 14 shows the voltage and currents for the SFS technique with $K_{SFS} = 0$ Hz^{-1} and VFP relay. When $K_{SFS} = 0$ Hz^{-1}, the critical detection time is $t = 132$ ms, noting that the SFS technique with $K_{SFS} = 0$ Hz^{-1} became in comportment like AFD method. Furthermore, the PV generator has lost its stability [102] at $K_{SFS} = 0.018$ Hz^{-1}, during which the islanding operation mode is quickly detected. Moreover, the islanding frequency reached the 60.5 Hz value over a longer period when $K_{SFS} =$ 0.05 Hz^{-1} [37]. Therefore, the system protection does not detect the islanding operating mode in all situations [37].

Similar anti-islanding tests were done for the SMS method with different θ_m values (25°, 15°, and 10°). Fig. 15 illustrates the islanding response of the PV system with SMS technique and VFP relay regarding the voltage V_{PCC}, current I_{PCC}, and fault signal only in the first $\theta_m = 25°$ condition.

Noted that for the other $\theta_m = 10°$ and $\theta_m = 15°$ conditions, the PCC frequency f_{PCC} decreased and became lower than the VFP set point after the power grid's disconnection [13]. Meanwhile, the PV inverter ceased supplying the local load within six cycles after the frequency exceeded the frequency's lower limits [13] at 783 ms and 285.8 ms, respectively (see Table 2). Therefore, the grid-connected PV converter is turned off. Furthermore, the PCC voltage V_{PCC} and PCC current I_{PCC} decreased to zero when the disconnecting signal was zero.

According to the IEEE 929–2000 standard [4], the most unfavorable situation happens when $Q_f = 2.5$, which is not verified for $\theta_m = 25°$ and verified when $\theta_m = 15°$ and $\theta_m = 10°$ Here the AFD phase angle φ_{inv_AFD} is always positive. On the other hand, the SMS and SFS phase angle, φ_{inv_SFS} and φ_{inv_SMS} can be positive or negative. The AFD inverter current is always a maximum frequency, whereas, for the SMS and SFS techniques, the current frequency drift can be up/down [13].

Fig. 16 depicts the PV system response for the SVS method with $K_{SVS} = 1$ A/V and VFP passive method in terms of V_{PCC} voltage, I_{PCC} current, disconnecting signal, and inverter shut-down time which are obtained the best islanding detection time of 428 ms.

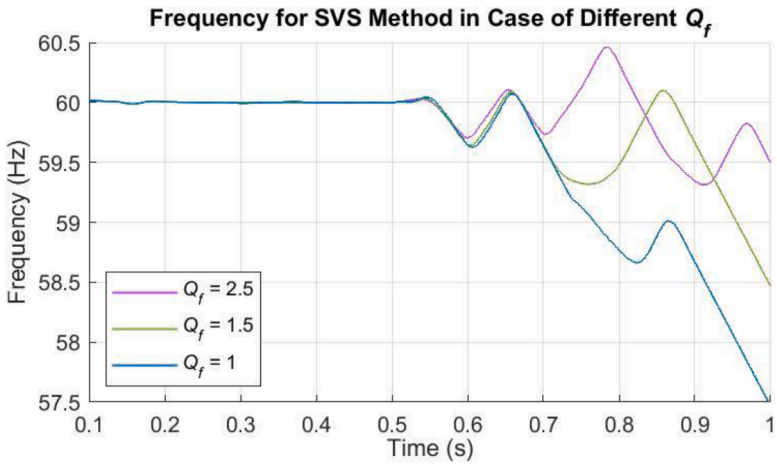

(a)

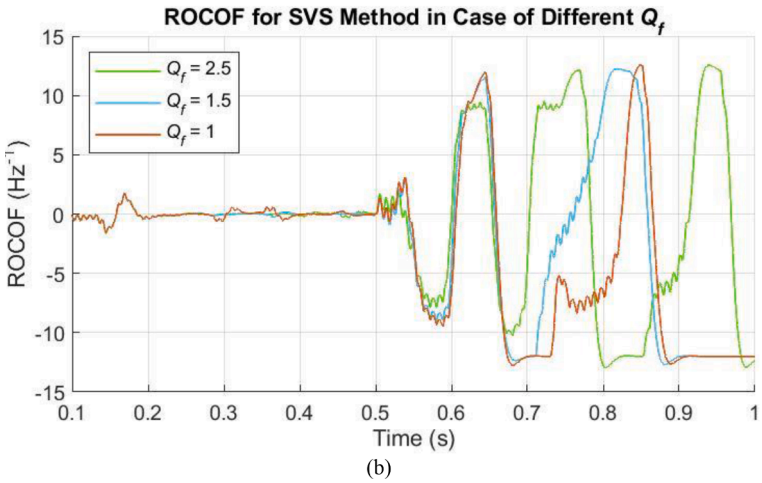

(b)

Fig. 23. SVS method for different Q_f. (a) Frequency. (b) ROCOF.

3. Simulation results and discussions

In this section, some case studies illustrate the islanding performances of the analyzed active methods under different quality factors, load types, irradiance changes, FRT operation mode, and effectiveness in hybrid strategies.

3.1. Simulation case studies

3.1.1. Different load quality factors

To evaluate that the studied active methods are effective under different standards requirements [35], the PV system is simulated under a Q_f range between 1 and 2.5 [24]. The obtained simulation results are depicted from Fig. 17 to Fig. 23. The quality and the perturbation given by the studied methods are presented by those graphics.

3.1.2. Different load types

The AFD voltage and frequency for different loads are represented in Fig. 24. In Fig. 25, the SFS voltage for different load types is shown. The SMS voltage and frequency in the case of different load types are described in Fig. 26. The SVS voltage and frequency for different kinds of loads are depicted in Fig. 27.

As can be observed from the obtained results, the effect of changing load types on the IDMs can be demonstrated by those figures, and to know if the active methods can support these forced changes in load in terms of detection time and the quality signal (The first limit for active methods is that they have a large perturbation in terms of signal quality.) against the used IEEE Std. 929 requirements.

3.1.3. Irradiation effect scenarios

The solar irradiation variation used in this study is shown in Fig. 28. The irradiation shape is not real but is used to show how fast the controller responds under the worst-case scenario. The solar irradiance does not change from 500 to 1000 W/m^2 in 0.1 s. It takes at least 8 s [103].

Considering the solar irradiation variation as depicted in Fig. 28, the PCC grid voltage and current of the studied active islanding methods for increasing and decreasing irradiance will be represented in Fig. 29. Fig. 30 illustrates the active and reactive power for increasing and decreasing in irradiance, while Fig. 31 shows the frequency and ROCOF for increasing and decreasing irradiance. From the obtained results, it can be concluded that studied IDMs perform very well under solar irradiation variations.

3.2. Performance of studied anti-islanding methods under fault-ride through

New grid requirements have been imposed on the IDMs. For example, because of stability and supportability issues, the PV inverters have been required to meet frequency and voltage FRT curves so that they cannot be disconnected under certain circumstances. This section discusses how the FRT requirements might adversely affect the

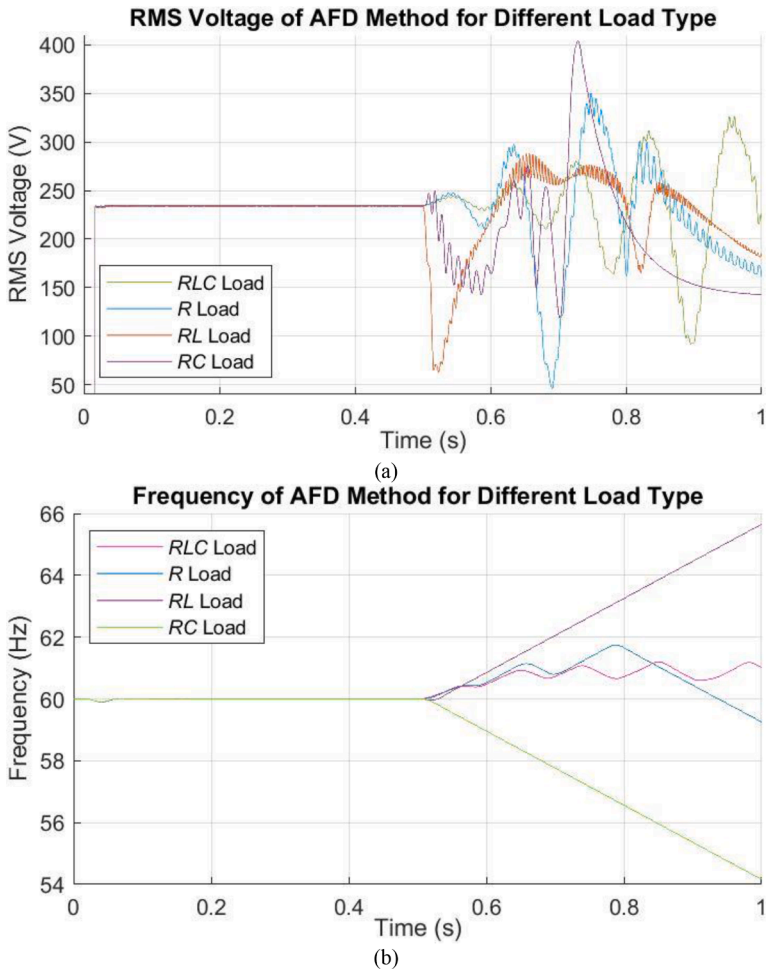

Fig. 24. AFD method for different kinds of loads. (a) Voltage. (b) Frequency.

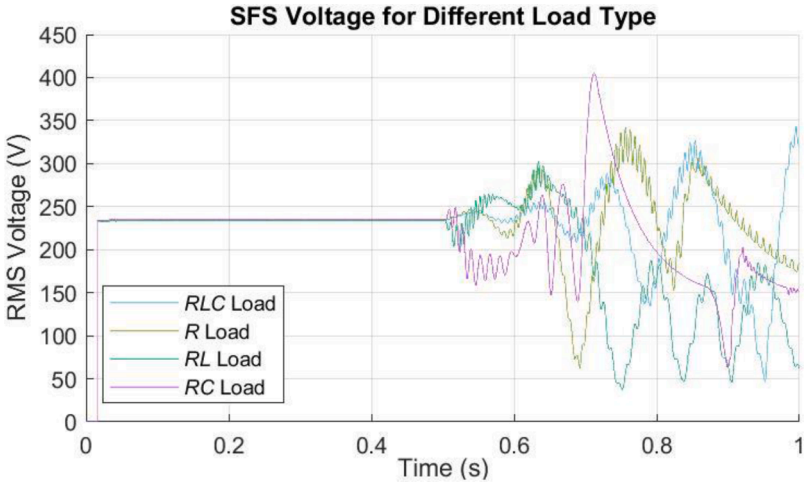

Fig. 25. RMS Voltage for SFS method in case of different load types.

performance of islanding detections.

The performance of the studied IDMs under FRT required by current grid codes is illustrated in Fig. 32. The considered scenarios under this case study are the behavior of each analyzed anti-islanding method under islanding with and without faults cases and fault without islanding case, respectively. As shown in Fig. 32, all studied active anti-islanding methods are effective during FRT. However, new requirements may appear in the future.

3.3. Evaluation effectiveness of active methods in hybrid strategies

From the above figures, can be observed and noted the effect of each studied active method. This section evaluates the analyzed active IDMs in a hybrid islanding detection strategy with passive methods from [34]

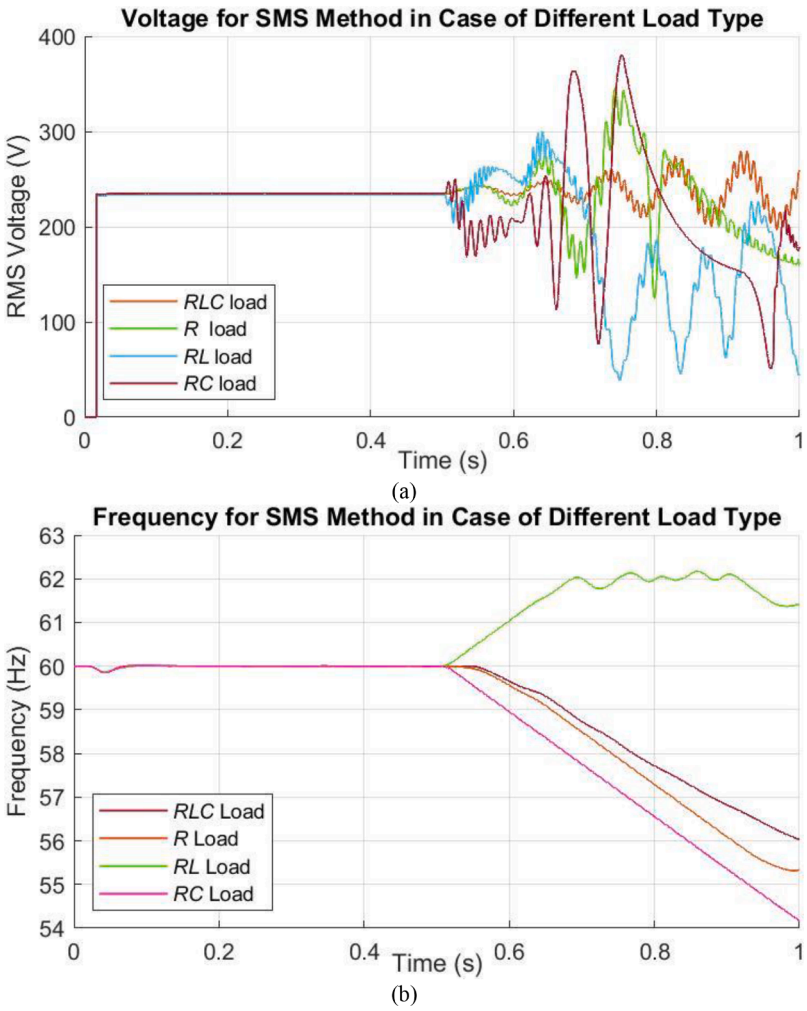

Fig. 26. SMS method for different kinds of loads. (a) Voltage. (b) Frequency.

concerning detection time. In the subsequent experiments, the PV system will be disconnected using VFP [13,34] and ROCOF [3,34] relays, respectively.

3.3.1. *Different quality factors scenario*

Table 3 shows the results for *RLC* load under islanding, at $Q_f = 1$, $Q_f = 1.5$, and $Q_f = 2.5$, respectively. The best detection for the VFP relay timing is registered for the case of SFS IDM with $Q_f = 1$ by 129.7 ms after the grid is disconnected. For the ROCOF relay timing, the best case was also for SFS IDM with $Q_f = 1$ and detection time of 117 ms.

3.3.2. *Different load types scenario*

The detection times of the analyzed active methods in the hybrid strategy [34] for different load types are given in Table 4.

For the scenario of different load types, the best cases are registered for VFP relay timing in the AFD method with *RL* load case (47.1 ms) and for the ROCOF passive relay timing in the AFD method with pure resistive load *R* case (20.4 ms). On the other hand, the most unfavorable result using the VFP passive method is registered for the SFS IDM with *RC* load by 539 ms. For ROCOF passive protection method timing, the worst-case scenario is for *RC* load too for AFD method by 631 ms. Otherwise, the results show some limitations: the ROCOF relay fails to detect the islanding mode for SFS IDM with *RC* load, and the VFP relay also fails to detect islanding mode for SMS IDM with *RC* load.

3.3.3. *Solar irradiation changes scenario*

The influence of the solar irradiation changes in the proposed hybrid strategies from [50] with analyzed active methods has been summarized in Table 5. In this table, the solar irradiation changes from Fig. 28 have been considered for all the active methods previously presented to determine the detection times of the hybrid method with VFP, and ROCOF relays from [34].

3.3.3.1. Solar irradiation decreasing. For the solar irradiation decreasing scenario, the best case for the VFP relay timing is SVS IDM with a 204 ms detection time; for the ROCOF relay timing, the best case was 133.4 ms recorded in the SVS method. Also, the worst case for VFP relay was obtained in the case of AFD method (342.8 ms), and the worst case for the ROCOF protection relay was in the case of SMS IDM (1.108 s).

3.3.3.2. Solar irradiation increasing. For the scenario of irradiation increasing, the SFS method gives the best performance by recording 148 ms in the VFP relay. For the ROCOF relay timing, the best detection time was also in the case of the SFS method (31.7 ms). The worst-case were the ones of the SVS (471.5 ms) and SMS (308.9 ms) IDMs for VFP and ROCOF relays, respectively.

3.4. *Discussion of obtained results and main achievements*

The existing and novel methods have been studied in this paper by

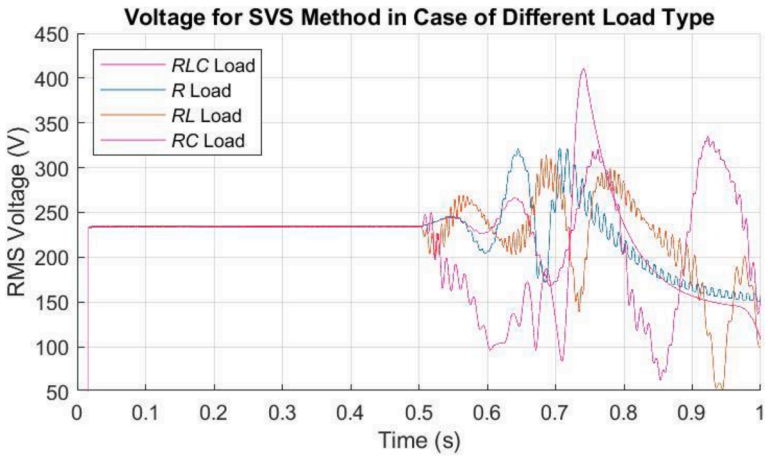

(a)

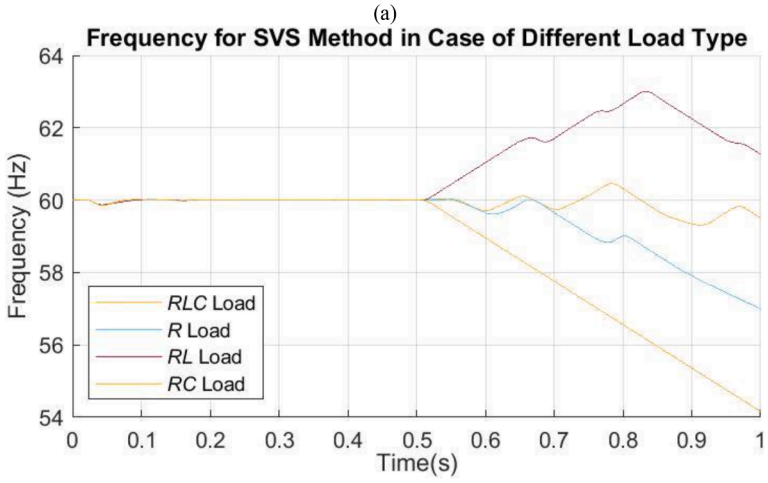

(b)

Fig. 27. SVS method for different kinds of loads. (a) Voltage. (b) Frequency.

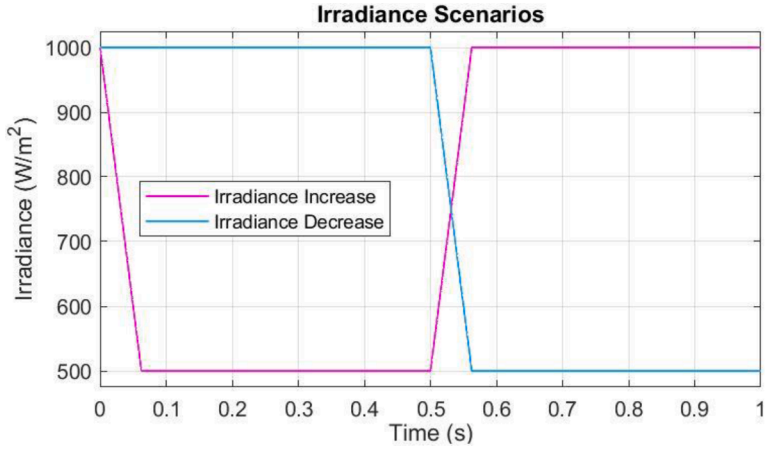

Fig. 28. Irradiation variation scenarios.

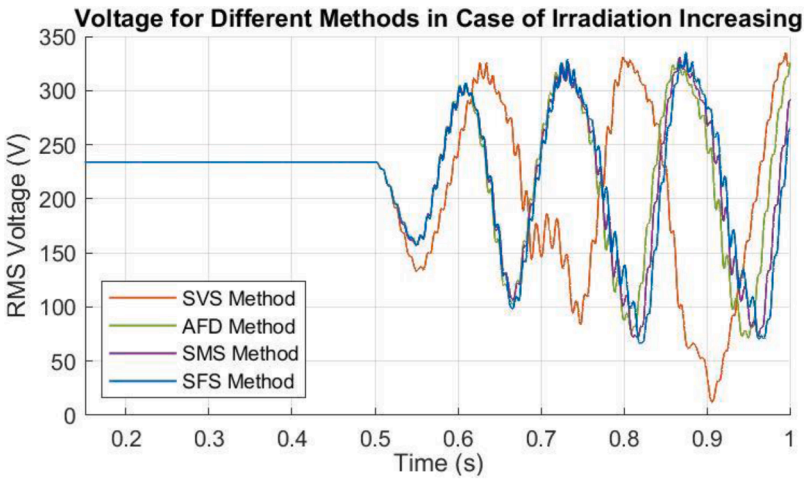

(a)

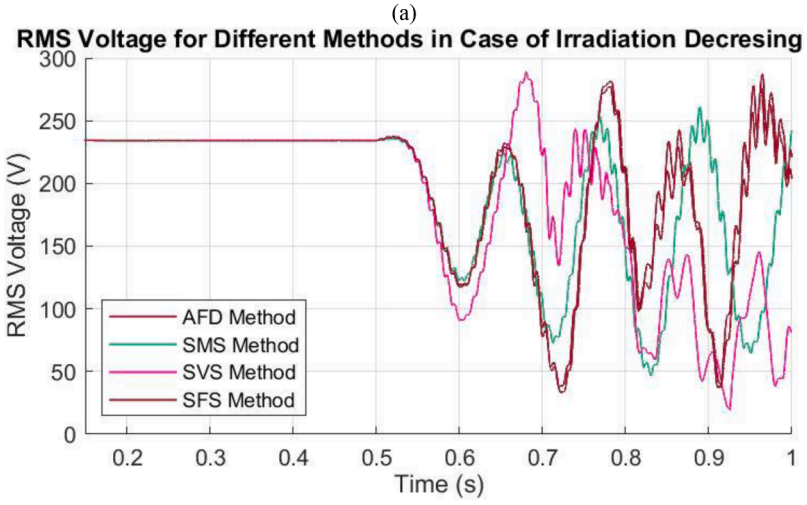

(b)

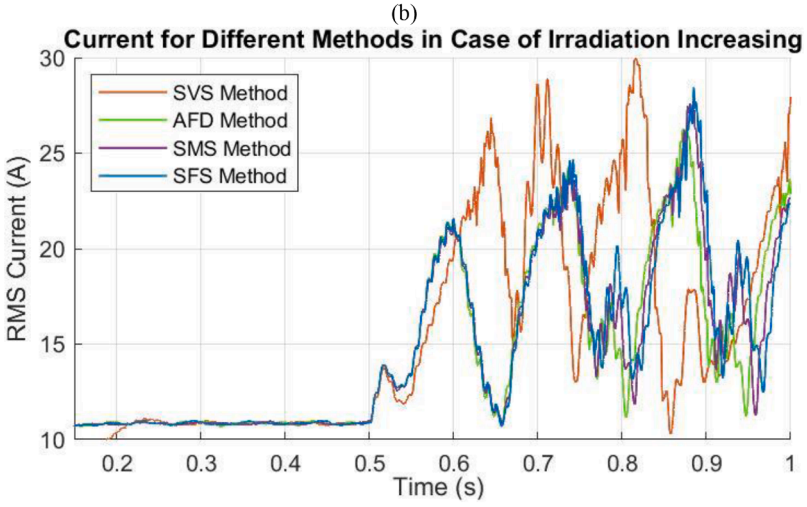

(c)

Fig. 29. Studied active islanding methods under solar irradiation variations. (a) RMS voltage for irradiance increasing. (b) RMS voltage for irradiance decreases. (c) RMS current for irradiance increases. (d) RMS current for irradiance decreases.

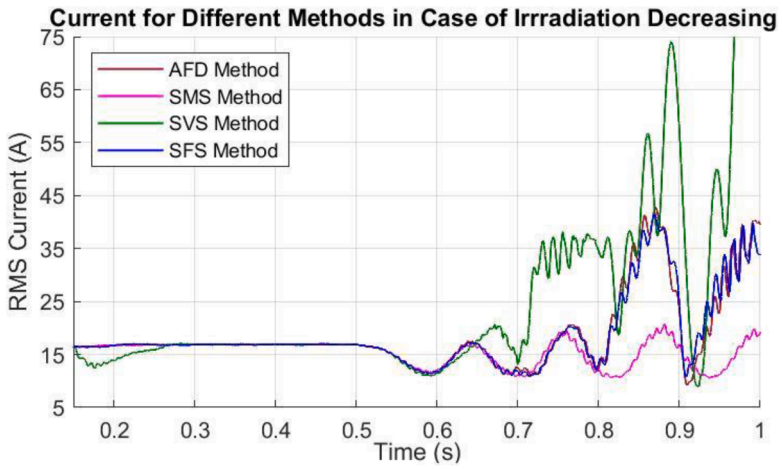

(d)

Fig. 29. (*continued*).

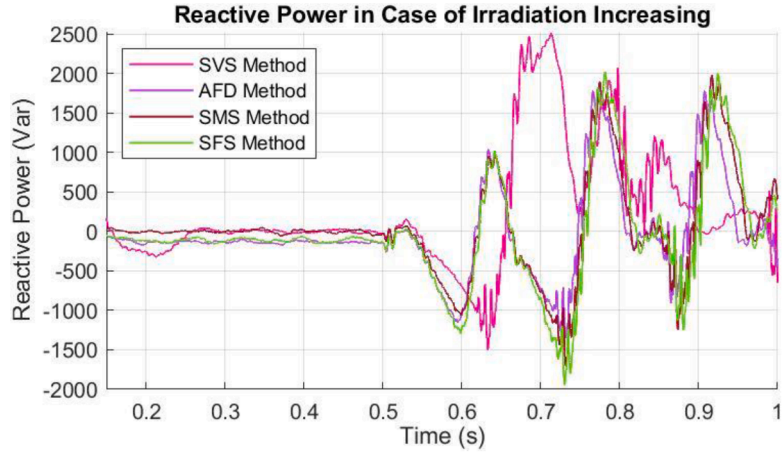

(a)

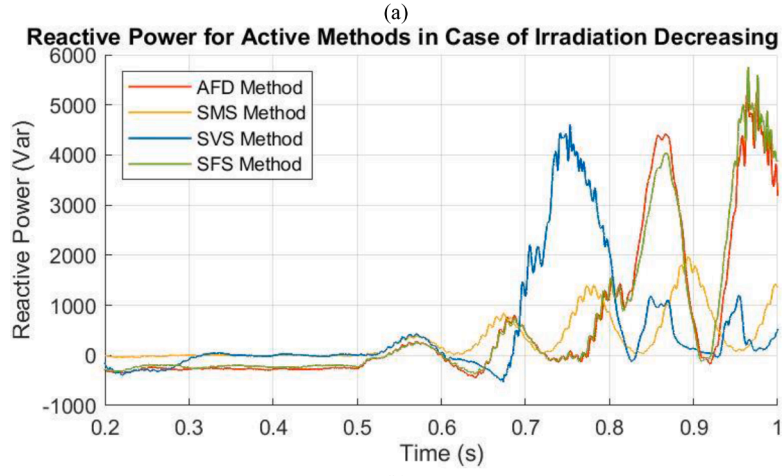

(b)

Fig. 30. Studied active islanding methods under solar irradiation variations. (a) Reactive power in case of irradiance increases. (b) Reactive power in case of irradiance decreases. (c) Active power for irradiance increasing. (d) Active power for irradiance decreases.

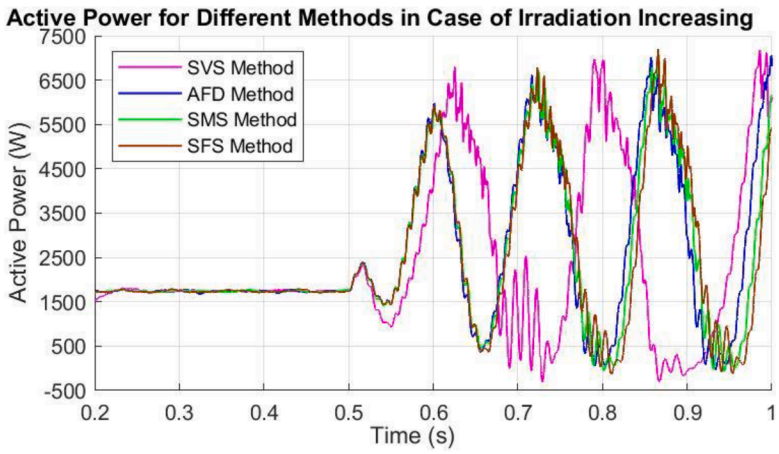

(c)

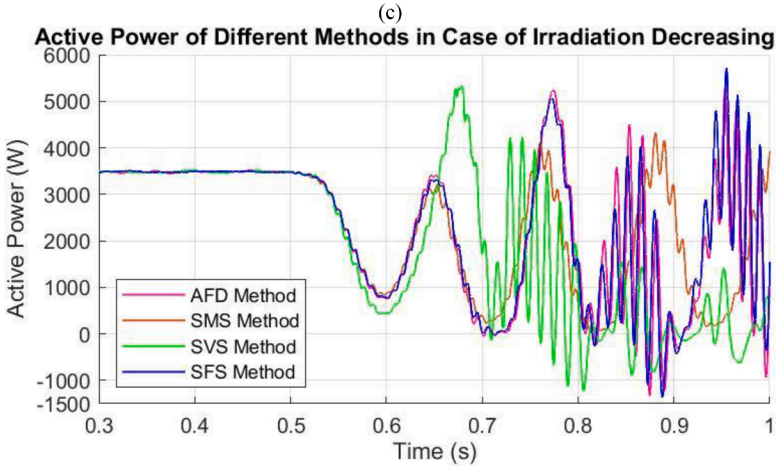

(d)

Fig. 30. (*continued*).

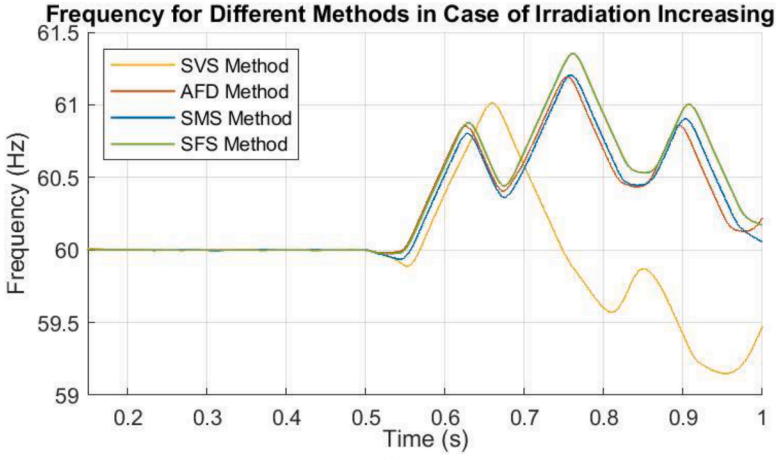

(a)

Fig. 31. Solar irradiance variations. (a) Frequency for solar irradiation increases. (b) Frequency for solar irradiation decreases. (c) ROCOF for solar irradiation increases. (d) ROCOF for solar irradiation decreasing.

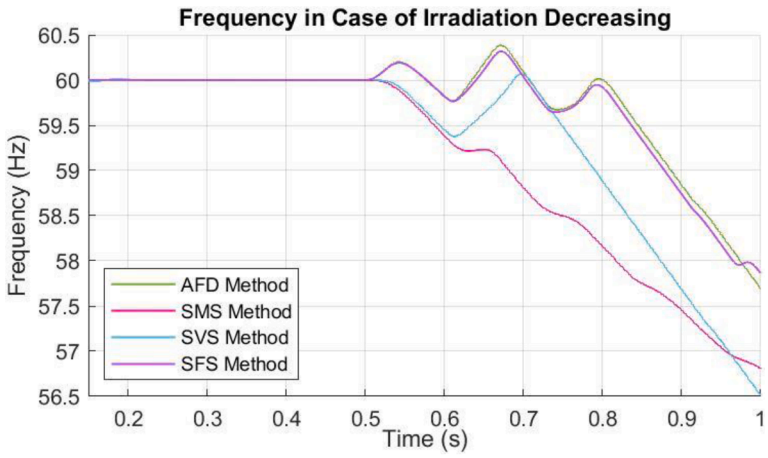

(b)

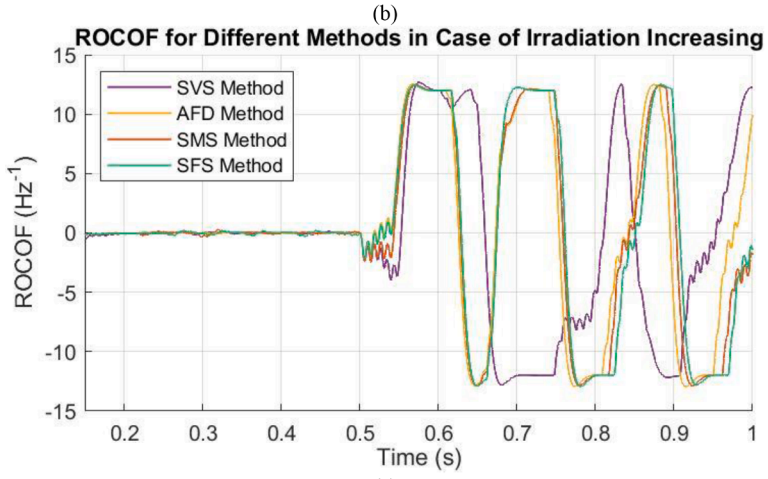

(c)

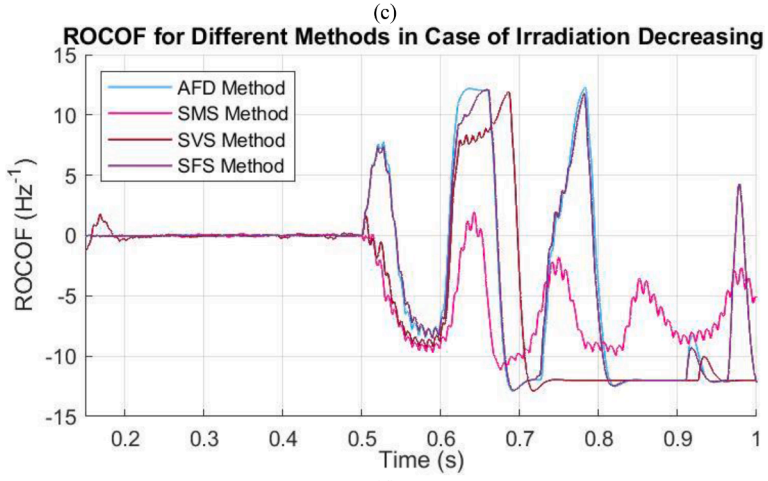

(d)

Fig. 31. (*continued*).

hybridizing them with classical VFP and other passive methods as ROCOF. That made it a novel and improved technique studied under different parameters and scenarios to show their performance and limitations.

The analyzed IDMs result in no fault detection zone (FDZ) [34,40]. The analyzed active methods have a low computational burden and operation time [39] compared with intelligent [16] and passive methods [6].

The studied active methods have good and acceptable power quality in terms of total harmonic distortion (THD) wherein some form of external perturbation or injection in terms of current, voltage, or phase angle is involved [34,86].

4. Conclusions

This paper discussed the implementation and performance evaluation under different case studies of four active IDMs: the AFD, SFS, SVS, and SMS methods. The testing system consisted of a single-phase grid-tied transformerless PV residential system, a single-phase DC-AC inverter, an inverter control with an MPPT controller, a utility grid, and a residential load. The UOV and UOF islanding protection methods, standard protections used for most grid-connected PV systems, were

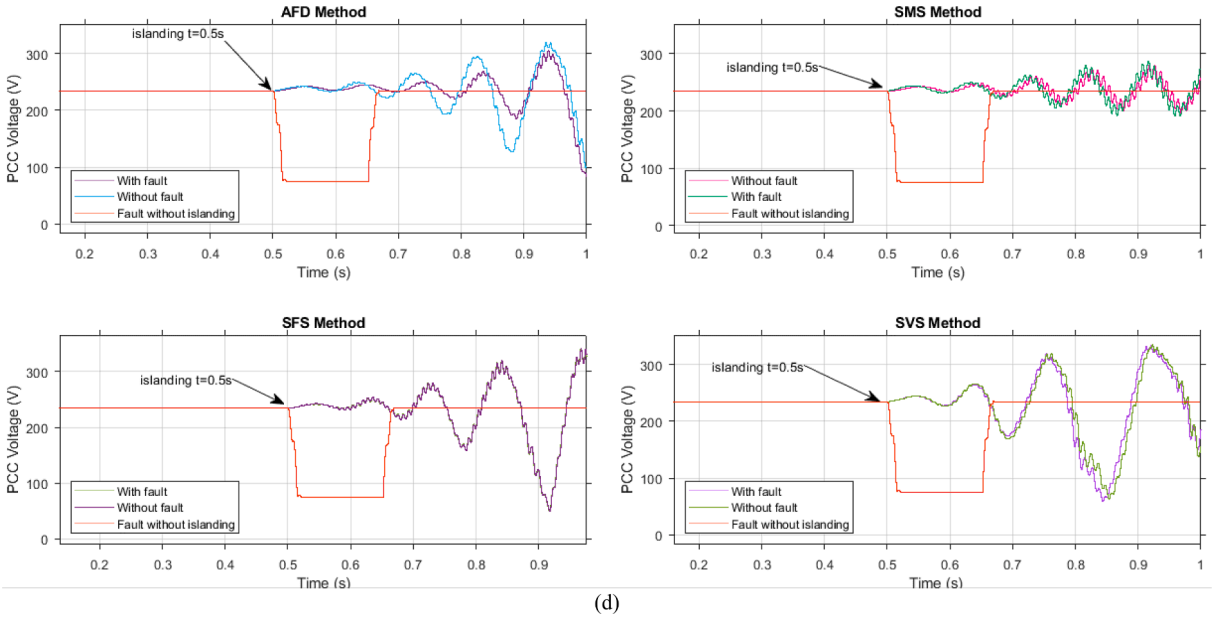

(d)

Fig. 32. Studied anti-islanding methods under FRT operation. (a) AFD method. (b) SMS method. (c) SFS method. (d) SVS method.

Table 3
Detection time in case of different quality factors scenario (ms). (a) VFP Relay. (b) ROCOF relay.

Active IDM	$Q_f = 2.5$	$Q_f = 1.5$	$Q_f = 1$
(a)			
AFD	132.0	131.5	131.2
SFS	131.0	130.5	129.7
SMS	220.2	121.5	205.4
SVS	436.0	292.1	222.0
(b)			
AFD	119.2	118.3	117.9
SFS	118.7	117.7	117.0
SMS	230.2	204.8	121.2
SVS	120.1	292.1	119.6

Table 4
Detection time for different load types scenario (ms). (a) VFP Relay. (b) ROCOF relay.

Active IDM	*RLC*	*R*	*RC*	*RL*
(a)				
AFD	132.0	74.6	145.3	47.1
SFS	131.0	74.4	539.0	59.0
SMS	220.2	127.3	–	59.0
SVS	436.0	133.0	514.0	59.5
(b)				
AFD	119.2	20.4	631.0	101.6
SFS	118.7	21.2	–	43.4
SMS	223.9	121.7	169.6	31.5
SVS	120.1	120.4	222.5	43.9

chosen as implicit islanding protection methods since they are simple and compatible with the analyzed PV system.

In this work, the most common anti-islanding methods are analyzed with a study in detail of their different actions when islanding occurs. Furthermore, the study covers the reaction of each method when hybridizing them with VFP and ROCOF passive methods because they are the best in terms of detection and sensibility. The study also included all methods in different parameters and in different scenarios to get a better conclusion. In addition, more simulation test cases considering different load quality factors, types of loads, solar irradiation effect conditions,

Table 5
Detection time for solar irradiation changes scenario (ms). (a) Solar irradiation decreasing. (b) Solar irradiation increasing.

Active IDM	VFP	ROCOF
(a)		
AFD	342.8	245.7
SFS	342.6	450.4
SMS	333.9	1108.0
SVS	204.0	133.4
(b)		
AFD	182.3	37.1
SFS	148.0	31.7
SMS	271.1	308.9
SVS	471.5	119.8

and FRT operation on each active IDM were added to sustain the obtained results. Finally, the active methods are studied and compared for the first time.

The conclusions of the studies can be drawn as follows:

(1) The detection time for the considered active methods satisfies the IEEE Std. 929–2000 and IEEE 1547.1 conditions verifying the 2 s requirement, sometimes the detection time was less than 1 s.
(2) The SFS method is better than the AFD method, demonstrated by detection time and quality signal results. However, the AFD and SFS IDMs have minor differences in results for different quality factors scenarios.
(3) The SVS active method has the longest VFP detection time because its VFP passive relay considers the 120 cycles required by the IEEE 929–2000 standard for the voltage relay, which take a long time to trip-off. This scenario does not happen in ROCOF passive relay because it does not take all this time. Thus, the ROCOF passive relay has a good detection time for the SVS active method and all active methods in all cases.
(4) The best detection time of islanding mode in the studied scenarios was detected in the SFS active method with ROCOF passive protection relay. However, the SFS method needed a more significant change in active power to detect the islanding operation mode. Therefore, the SMS islanding technique is recommended for grid-tied PV power systems because it gives the best detection time and signal quality with less deterioration.

(5) The analyzed active methods detect islanding mode effectively and effortlessly under different quality factors, types of loads, solar irradiation changes, and FRT operation mode. Moreover, those methods can effectively work in hybrid IDMs with passive methods like VFP and ROCOF.

Declaration of Competing Interest

The authors declare that they have no known competing financial interests or personal relationships that could have appeared to influence the work reported in this paper.

Acknowledgements

This work was supported by VILLUM FONDEN under the VILLUM Investigator Grant (no. 25920): Center for Research on Microgrids (CROM); www.crom.et.aau.dk.

References

[1] S.S. Mohapatra, M.K. Maharana, S.B. Pati, Comprehensive review to analyze the islanding in distributed generation system, in: 2021 1*st Int. Conf. Power Electron. and Energy (ICPEE)*, 2021, pp. 1–7, https://doi.org/10.1109/ICPEE50452.2021.9358542.

[2] S.B. Jinjala, B.N. Vaidya, Analysis of active and passive method for islanding detection of 3-phase grid connected PV system, in: 2*nd Int. Conf. Trends Electron. and Inform. (ICOEI)*, Tirunelveli, 2018, pp. 592–597, https://doi.org/10.1109/ICOEI.2018.8553862.

[3] I.V. Banu, M. Istrate, Islanding prevention scheme for grid-connected photovoltaic systems in Matlab/Simulink, in: 49*th Int. Universities Power Eng. Conf. (UPEC)*, Cluj-Napoca, Romania, 2014, pp. 1–6, https://doi.org/10.1109/UPEC.2014.6934698.

[4] *IEEE recommended practice for utility interface of photovoltaic (PV) systems*, IEEE Std. 929-2000, 2000, doi:10.1109/IEEESTD.2000.91304 .

[5] R. Teodorescu, M. Liserre, and P. Rodriguez, "Grid converters for photovoltaic and wind power systems," Chichester: John Wiley & Sons, Ltd, 2011, doi: 10.1002/9780470667057.

[6] V.R. Reddy, E.S. Sreeraj, a feedback-based passive islanding detection technique for one-cycle-controlled single-phase inverter used in photovoltaic systems, IEEE Trans. Ind. Electron. 67 (8) (2020) 6541–6549, https://doi.org/10.1109/TIE.2019.2938464.

[7] G. Bayrak, A remote islanding detection and control strategy for photovoltaic-based distributed generation systems, Energy Convers. Manag. 96 (2015) 228–241, https://doi.org/10.1016/J.ENCONMAN.2015.03.004.

[8] D. Rebollal, M. Carpintero-Rentería, D. Santos-Martín, M. Chinchilla, Microgrid and distributed energy resources standards and guidelines review: grid connection and operation technical requirements, Energies 14 (3) (2021) 523, https://doi.org/10.3390/en14030523.

[9] I.V. Banu, M. Istrate, D. Machidon, R. Pantelimon, A study on anti-islanding detection algorithms for grid-tied photovoltaic systems, in: *Int. Conf. Optimization Elect. and Electron. Equipment (OPTIM)*, Brasov, Romania, 2014, pp. 655–660, https://doi.org/10.1109/OPTIM.2014.6850940.

[10] K. Arulkumar, D. Vijayakumar, K. Palanisamy, Recent advances and control techniques in grid-connected PV system–a review, Int. J. Renew. Energy Res. 6 (3) (2016) 1037–1049, https://doi.org/10.20508/ijrer.v6i3.4075.g6886.

[11] A. Eltawil, Z. Zhao, Grid-connected photovoltaic power systems: technical and potential problems—a review, Renew. Sustain. Energy Rev. 14 (1) (2010) 112–129, https://doi.org/10.1016/J.RSER.2009.07.015.

[12] W.J. Chiang, H.L. Jou, J.C. Wu, K.D. Wu, Y.T. Feng, Active islanding detection method for the grid-connected photovoltaic generation system, Electr. Power Syst. Res. 80 (4) (2010) 372–379, https://doi.org/10.1016/j.epsr.2009.09.018.

[13] A. Lopes, H. Sun, Performance assessment of active frequency drifting islanding detection methods, IEEE Trans. Energy Convers. 21 (1) (Mar. 2006) 171–180, https://doi.org/10.1109/TEC.2005.859981.

[14] H. Karimi, A. Yazdani, R. Iravani, Negative-sequence current injection for fast islanding detection of a distributed resource unit, IEEE Trans. Power Electron. 23 (1) (Jan. 2008) 298–307, https://doi.org/10.1109/TPEL.2007.911774.

[15] M. Al Hosani, Z. Qu, H.H. Zeineldin, A transient stiffness measure for islanding detection of multi-DG systems, IEEE Trans. Power Del. 30 (2) (Apr. 2015) 986–995, https://doi.org/10.1109/TPWRD.2014.2360876.

[16] M.S. Kim, R. Haider, G.J. Cho, C.H. Kim, C.Y. Won, J.S. Chai, Comprehensive review of islanding detection methods for distributed generation systems, Energies 12 (5) (Mar. 2019) 837, https://doi.org/10.3390/en12050837.

[17] M.A. Khan, A. Haque, V.S. Bharath Kurukuru, M. Saad, Islanding detection techniques for grid-connected photovoltaic systems-a review, Renew. Sustain. Energy Rev. 154 (2022), 111854, https://doi.org/10.1016/j.rser.2021.111854. ISSN 1364-0321.

[18] N. Gupta, R. Dogra, R. Garg, P. Kumar, Review of islanding detection schemes for utility interactive solar photovoltaic systems, Int. J. Green Energy 19 (3) (2022) 242–253, https://doi.org/10.1080/15435075.2021.1941048.

[19] A. Hussain, C.H. Kim, A. Mehdi, A comprehensive review of intelligent islanding schemes and feature selection techniques for distributed generation system, IEEE Access 9 (2021) 146603–146624, https://doi.org/10.1109/ACCESS.2021.3123382.

[20] B. K.Panigrahi, A. Bhuyan, J. Shukla, P.K. Ray, S. Pati, A comprehensive review on intelligent islanding detection techniques for renewable energy integrated power system, Int. J. Energy. Res. 45 (2021) 14085–14116, https://doi.org/10.1002/er.6641.

[21] S. Raza, H. Arof, H. Mokhlis, H. Mohamad, H.A. Illias, Passive islanding detection technique for synchronous generators based on performance ranking of different passive parameters, IET Gener. Transm. Distrib. 11 (17) (2017) 4175–4183, https://doi.org/10.1049/IET-GTD.2016.0806.

[22] Q. Sun, J.M. Guerrero, T. Jing, J.C. Vasquez, R. Yang, An islanding detection method by using frequency positive feedback based on FLL for single-phase microgrid, IEEE Trans. Smart Grid 8 (4) (2017) 1821–1830, https://doi.org/10.1109/TSG.2015.2508813.

[23] B. Yu, M. Matsui, G. Yu, A review of current anti-islanding methods for photovoltaic power system, Solar Energy 84 (5) (2010) 745–754.

[24] M. Aman, B. Jasmon, B. Mokhlis, A. Khan, A. Bakar, M. Karimi, Modeling and simulation of digital frequency relay for generator protection, in: IEEE Int. Conf. Power and Energy, 2012, pp. 701–706, https://doi.org/10.1109/PECON.2012.6450305.

[25] Y.A. Elshrief, D.H. Helmi, S. Abd-Elhaleem, B.A. Abozalam, A.D. Asham, Fast and accurate islanding detection technique for microgrid connected to photovoltaic system, J. Radiat. Res. Appl. Sci. 14 (1) (2021) 210–221, https://doi.org/10.1080/16878507.2021.1923913.

[26] *IEEE standard for interconnecting distributed resources with electric power systems*, IEEE std. 1547–2003, Jul. 2003, doi: 10.1109/IEEESTD.2003.94285.

[27] X. Li, R.S. Balog, Analysis and comparison of two active anti-islanding detection methods, in: 2014 *IEEE* 57*th Int. Midwest Symp. Circuits and Systems (MWSCAS)*, 2014, pp. 443–446, https://doi.org/10.1109/MWSCAS.2014.6908447.

[28] J. Laghari, H. Mokhlis, A. Bakar, M. Karimi, A new islanding detection technique for multiple mini hydro based on rate of change of reactive power and load connecting strategy, Energy Convers. Manag. 76 (2013) 215–224, https://doi.org/10.1016/J.ENCONMAN.2013.07.033.

[29] Z. Ye, A. Kolwalkar, Y. Zhang, P. Du, R. Walling, Evaluation of anti-islanding schemes based on nondetection zone concept, IEEE Trans. Power Electron. 19 (5) (Sept. 2004) 1171–1176, https://doi.org/10.1109/TPEL.2004.833436.

[30] J. Estébanez, M. Moreno, A. Pigazo, M. Liserre, A. Dell'Aquila, Performance evaluation of active islanding-detection algorithms in distributed-generation photovoltaic systems: two inverters case, IEEE Trans. Ind. Electron. 58 (4) (2011) 1185–1193, https://doi.org/10.1109/TIE.2010.2044132.

[31] P. Kumar, A. Shukla, S. Anand, S. Pundir, S. Sarkar, A modified SMS islanding detection technique for reduced non detection zone, 20th Eur. Conf. Power Electron. and Appl., Riga (2018) P.1–P.9.

[32] A.G. AboKhalil, A.B. Awan, A.R. Al-Qawasmi, Comparative study of passive and active islanding detection methods for PV grid-connected systems, Sustainability 10 (6) (2018) 1798, https://doi.org/10.3390/SU10061798.

[33] T. Rabuzin, F. Hohn, L. Nordström, Computation of sensitivity-based islanding detection parameters for synchronous generators, Electr. Power Syst. Res. 190 (2021), https://doi.org/10.1016/j.epsr.2020.106611.

[34] Fadila Barkat, A. Cheknane, J.M. Guerrero, A. Lashab, M. Istrate, I.V. Banu, Hybrid islanding detection technique for single-phase grid-connected photovoltaic multi-inverter systems, IET Renew. Power Generation (20 Jan. 2021), https://doi.org/10.1049/iet-rpg.2019.1183. ISSN 1752-1416.

[35] R. Bakhshi, S. Javad, Voltage positive feedback based active method for islanding detection of photovoltaic system with string inverter using sliding mode controller, Solar Energy 137 (2016) 564–577, https://doi.org/10.1016/J.SOLENER.2016.08.051.

[36] R. Bakhshi-Jafarabadi, R. Ghazi, J. Sadeh, Power quality assessment of voltage positive feedback based islanding detection algorithm, J. Modern Power Syst. Clean Energy 8 (4) (July 2020) 787–795, https://doi.org/10.35833/MPCE.2018.000509.

[37] X. Wang, W. Freitas, W. Xu, Dynamic non-detection zones of positive feedback anti-islanding methods for inverter-based distributed generators, IEEE Trans. Power Del. 26 (2) (2011) 1145–1155, https://doi.org/10.1109/TPWRD.2010.2090672.

[38] E. Kamyab, J. Sadeh, Islanding detection method for photovoltaic distributed generation based on voltage drifting, IET Gener. Transm. Distrib. 7 (6) (2013) 584–592, https://doi.org/10.1049/IET-GTD.2012.0507.

[39] D. Mlakić, H.R. Baghaee, S. Nikolovski, A novel ANFIS-based islanding detection for inverter-interfaced microgrids, IEEE Trans. Smart Grid 10 (4) (2019) 4411–4424, https://doi.org/10.1109/TSG.2018.2859360.

[40] H.R. Baghaee, D. Mlakić, S. Nikolovski, T. Dragicčvić, Anti-islanding protection of PV-based microgrids consisting of PHEVs using SVMs, IEEE Trans. Smart Grid 11 (1) (Jan. 2020) 483–500, doi:.

[41] A. Serrano-Fontova, J.A. Martinez, P. Casals-Torrens, R. Bosch, A robust islanding detection method with zero-non-detection zone for distribution systems with DG, Int. J. Electr. Power Energy Syst. 133 (2021), 107247, https://doi.org/10.1016/j.ijepes.2021.107247. ISSN 0142-0615.

[42] M. Seyedi, S.A. Taher, B. Ganji, J.M. Guerrero, A hybrid islanding detection method based on the rates of changes in voltage and active power for the multi-inverter systems, IEEE Trans. Smart Grid 12 (4) (2021) 2800–2811, https://doi.org/10.1109/TSG.2021.3061567.

[43] B.K. Chaitanya, A. Yadav, M. Pazoki, Reliable islanding detection scheme for distributed generation based on pattern-recognition, IEEE Trans. Ind. Informat. 17 (8) (2021) 5230–5238, https://doi.org/10.1109/TII.2020.3029675.

[44] P. Kumar, V. Kumar, B. Tyagi, Sequence-based hybrid technique for islanding detection for microgrid with RES, IEEE Trans. Ind. Appl. 58 (1) (2022) 185–200, https://doi.org/10.1109/TIA.2021.3130214.

[45] S. Mondal, P.K. Gayen, D.N. Gaonkar, Battery storage-based novel hybrid islanding detection technique using Lissajous pattern estimation, IEEE Trans. Instrum. Meas. 71 (2022) 1–11, https://doi.org/10.1109/TIM.2022.3169527. Art no. 9003711.

[46] X. Kong, X. Xu, Z. Yan, S. Chen, H. Yang, D. Han, Deep learning hybrid method for islanding detection in distributed generation, Appl. Energy 210 (2018) 776–785, https://doi.org/10.1016/J.APENERGY.2017.08.014.

[47] A. Esmaeilian, M. Kezunovic, Prevention of power grid blackouts using intentional islanding scheme, IEEE Trans. Ind. Appl. 53 (1) (2017) 622–629, https://doi.org/10.1109/TIA.2016.2614772.

[48] S. Raza, H. Mokhlis, H. Arof, J. Laghari, L. Wang, Application of signal processing techniques for islanding detection of distributed generation in distribution network: a review, Energy Convers. Manag. 96 (2015) 613–624, https://doi.org/10.1016/J.ENCONMAN.2015.03.029.

[49] J.A. Laghari, H. Mokhlis, M. Karimi, A.H.A. Bakar, Hasmaini Mohamad, Computational Intelligence based techniques for islanding detection of distributed generation in distribution network: a review, Energy Convers. Manag. 88 (2014) 139–152, https://doi.org/10.1016/J.ENCONMAN.2014.08.024.

[50] A. Khamis, H. Shareef, A. Mohamed, E. Bizkevelci, Islanding detection in a distributed generation integrated power system using phase space technique and probabilistic neural network, Neurocomputing 148 (2015) 587–599, https://doi.org/10.1016/j.neucom.2014.07.004.

[51] H. Shayeghi, B. Sobhani, Zero NDZ assessment for anti-islanding protection using wavelet analysis and neuro-fuzzy system in inverter based distributed generation, Energy Convers. Manag. 79 (2014) 616–625, https://doi.org/10.1016/J.ENCONMAN.2013.12.062.

[52] E. Ropp, M. Begovic, A. Rohatgi, Analysis and performance assessment of the active frequency drift method of islanding prevention, IEEE Trans. Energy Convers. 14 (3) (1999) 810–816, https://doi.org/10.1109/60.790956.

[53] M. Xu, V. Melnik, U. Borup, Modeling anti-islanding protection devices for photovoltaic systems, Renew. Energy 29 (15) (2004) 2195–2216, https://doi.org/10.1016/J.RENENE.2004.04.005.

[54] The MathWorks, Inc., "Single-phase, 240 Vrms, 3500W transformerless grid-connected PV array", Matlab 2020a, https://www.mathworks.com/help/physmod/sps/examples/single-phase-240-vrms-3500-w-transformerless-grid-connected-pv-array.html, accessed 22 September 2020.

[55] M.Y. Worku, M.A. Hassan, L.S. Maraaba, M.A. Abido, Islanding detection methods for microgrids: a comprehensive review, Mathematics 9 (24) (Dec. 2021) 3174–3196, https://doi.org/10.3390/math9243174 [Online]. Available:.

[56] Fadila Barkat, Performance evaluation of some active anti-islanding methods, IEEE Dataport (February 8, 2022), https://doi.org/10.21227/067m-d536.

[57] Z. Ye, R. Walling, L. Garces, R. Zhou, L. Li, T. Wang, Study and development of anti-islanding control for grid-connected inverters, Nat. Renew. Energy Laboratory, Tech. Rep. (May 2004), https://doi.org/10.2172/15007704. NREL/SR-560-36243.

[58] D. Voglitsis, N.P. Papanikolaou, A.C. Kyritsis, Active cross-correlation anti-islanding scheme for PV module-integrated converters in the prospect of high penetration levels and weak grid conditions, IEEE Trans. Power Electron. 34 (3) (March 2019) 2258–2274, https://doi.org/10.1109/TPEL.2018.2836663.

[59] D. Voglitsis, N. Papanikolaou, A.C. Kyritsis, Incorporation of harmonic injection in an interleaved flyback inverter for the implementation of an active anti-islanding technique, IEEE Trans. Power Electron. 32 (11) (Nov. 2017) 8526–8543, https://doi.org/10.1109/TPEL.2016.2646419.

[60] A.M.I. Mohamad, Y.A.I. Mohamed, Analysis and mitigation of interaction dynamics in active DC distribution systems with positive feedback islanding detection schemes, IEEE Trans. Power Electron. 33 (3) (March 2018) 2751–2773, https://doi.org/10.1109/TPEL.2017.2699233.

[61] A.M.I. Mohamad, Y.A.I. Mohamed, Impedance-based analysis and stabilization of active DC distribution systems with positive feedback islanding detection schemes, IEEE Trans. Power Electron. 33 (11) (Nov. 2018) 9902–9922, https://doi.org/10.1109/TPEL.2018.2790945.

[62] J. Muñoz-Cruzado-Alba, J. Villegas-Núñez, J.A. Vite-Frías, J.M. Carrasco-Solís, E. Galván-Díez, New low-distortion *Q–f* droop plus correlation anti-islanding detection method for power converters in distributed generation systems, IEEE Trans. Ind. Electron. 62 (8) (Aug. 2015) 5072–5081, https://doi.org/10.1109/TIE.2015.2405894.

[63] A. Cardenas, K. Agbossou, Experimental evaluation of voltage positive feedback based anti-islanding algorithm: multi-inverter case, IEEE Trans. Energy Convers. 27 (2) (June 2012) 498–506, https://doi.org/10.1109/TEC.2012.2188529.

[64] A. Yafaoui, B. Wu, S. Kouro, Improved active frequency drift anti-islanding detection method for grid connected photovoltaic systems, IEEE Trans. Power Electron. 27 (5) (May 2012) 2367–2375, https://doi.org/10.1109/TPEL.2011.2171997.

[65] A.Y. Hatata, El-H. Abd-Raboh, Bishoy, E. Sedhom, Proposed Sandia frequency shift for anti-islanding detection method based on artificial immune system, Alex. Eng. J. 57 (1) (2018) 235–245, https://doi.org/10.1016/j.aej.2016.12.020.

[66] L.P. Sampaio, M.A.G. de Brito, G. de A. E Melo, C.A. Canesin, Grid-tie three-phase inverter with active power injection and reactive power compensation, Renew. Energy 85 (2016) 854–864, https://doi.org/10.1016/j.renene.2015.07.034.

[67] B.I. Rani, M. Srikanth, G.S. Ilango, C. Nagamani, An active islanding detection technique for current controlled inverter, Renew. Energy 51 (2013) 189–196, https://doi.org/10.1016/j.renene.2012.09.019.

[68] B.Y. Yu, M.H. Matsui, Y.S. Jung, G.J. Yu, A combined active anti-islanding method for photovoltaic systems, Renew. Energy 33 (5) (2008) 979–985, https://doi.org/10.1016/j.renene.2007.06.012.

[69] S. Shrivastava, S. Jain, R.K. Nema, V. Chaurasia, Two level islanding detection method for distributed generators in distribution networks, Int. J. Electr. Power Energy Syst. 87 (2017) 222–231, https://doi.org/10.1016/j.ijepes.2016.10.009.

[70] A. Samui, S.R. Samantaray, An active islanding detection scheme for inverter-based DG with frequency dependent ZIP–exponential static load model, Int. J. Electr. Power Energy Syst. 78 (2016) 41–50, https://doi.org/10.1016/j.ijepes.2015.11.054.

[71] E. Vazquez, N. Vazquez, R. Femat, Modified Sandia voltage shift anti-islanding scheme for distributed power generator systems, IET Power Electron. 13 (18) (2020) 4226–4234, https://doi.org/10.1049/iet-pel.2020.0735.

[72] F. Valsamas, D. Voglitsis, N. Rigogiannis, N. Papanikolaou, A. Kyritsis, Comparative study of active anti-islanding schemes compatible with MICs in the prospect of high penetration levels and weak grid conditions, IET Gener. Transm. Distrib. 12 (20) (2018) 4589–4596, https://doi.org/10.1049/iet-pel.2020.0735.

[73] C.R. Aguiar, G. Fuzato, Guilherme, R.F. Bastos, A.F.Q Gonçalves, R.Q. Machado, Hybrid fuzzy anti-islanding for grid-connected and islanding operation in distributed generation systems, IET Power Electron. 9 (3) (2016) 512–518, https://doi.org/10.1049/iet-pel.2014.0717.

[74] C.C. Hou, Y.C. Chen, Active anti-islanding detection based on pulse current injection for distributed generation systems, IET Power Electron. 6 (8) (2013) 1658–1667, https://doi.org/10.1049/iet-pel.2012.0542.

[75] F.J. Lin, Y.S. Huang, K.H. Tan, J.H. Chiu, Y.R. Chang, Active islanding detection method using *D*-axis disturbance signal injection with intelligent control, IET Gener. Transm. Distrib. 7 (5) (2013) 537–550, https://doi.org/10.1049/iet-gtd.2012.0488.

[76] S. Khanbabapour, M.E. Hamedani Golshan, Synchronous DG planning for simultaneous improvement of technical, overcurrent, and timely anti-islanding protection indices of the network to preserve protection coordination, IEEE Trans. Power Del. 32 (1) (Feb. 2017) 474–483, https://doi.org/10.1109/TPWRD.2016.2538799.

[77] M. Khodaparastan, H. Vahedi, F. Khazaeli, H. Oraee, A novel hybrid islanding detection method for inverter-based DGs using SFS and ROCOF, IEEE Trans. Power Del. 32 (5) (Oct. 2017) 2162–2170, https://doi.org/10.1109/TPWRD.2015.2406577.

[78] O. Raipala, A. Mäkinen, S. Repo, and P. Järventausta, "An anti-islanding protection method based on reactive power injection and ROCOF," *IEEE Trans. Power Del.*, vol. 32, no. 1, pp. 401–410, Feb. 2017, doi: 10.1109/TPWRD.2016.2543503.

[79] B. Bahrani, H. Karimi, R. Iravani, Nondetection zone assessment of an active islanding detection method and its experimental evaluation, IEEE Trans. Power Del. 26 (2) (April 2011) 517–525, https://doi.org/10.1109/TPWRD.2009.2036016.

[80] G. Hernandez-Gonzalez, R. Iravani, Current injection for active islanding detection of electronically-interfaced distributed resources, IEEE Trans. Power Del. 21 (3) (July 2006) 1698–1705, https://doi.org/10.1109/TPWRD.2006.876980.

[81] I.J. Balaguer-Álvarez, E.I. Ortiz-Rivera, Survey of distributed generation islanding detection methods, IEEE Latin America Trans 8 (5) (2010) 565–570, https://doi.org/10.1109/TLA.2010.5623510.

[82] B. Yu, An improved active frequency drift anti-islanding method for multiple PV micro-inverter systems, IEICE Electron. Express 11 (6) (2014) 0143–2014, https://doi.org/10.1587/elex.11.20140143.

[83] M.R. Oshiro, R. Barros Godoy, M.A.G. de Brito, L. Galotto, Performance analysis of active anti-islanding techniques for photovoltaic application, in: 2019 *IEEE 15th Brazilian Power Electronics Conference and 5th IEEE Southern Power Electronics Conference (COBEP/SPEC)*, 2019, pp. 1–6, https://doi.org/10.1109/COBEP/SPEC44138.2019.9065606. Santos, Brazil.

[84] Y. Hong, W. Huang, Investigation of frequency drift methods of islanding detection with multiple PV inverters, in: Int. Conf. and Exp. Electron. and Appl., 2014, pp. 429–434, https://doi.org/10.1109/PEAC.2014.7037894.

[85] Fadila Barkat, A. Cheknane, Assessment of non-detection zone of different active anti-islanding methods for single and multi-inverters grid connected photovoltaic power systems, J. Sci. Eng. Sci. (Revue des Sci. et Sci. de l'ingénieur, RSSI) 7 (1) (Jun 2019) 34–43.

[86] El-Moubarak Mageda, H. Mahmoud, F. Ayman, Performance of three islanding detection methods for grid-tied multi-inverters, in: 2015 *IEEE 15th Int. Conf. Environment and Elect. Eng. (EEEIC)*, Rome, 2015, pp. 1999–2004, https://doi.org/10.1109/EEEIC.2015.7165481, 2015.

[87] P. Sanchis, L. Marroyo, J. Coloma, Design methodology for the frequency shift method of islanding prevention and analysis of its detection capability, Prog. Photovolt: Res. Appl. 13 (Apr. 2005) 409–428, https://doi.org/10.1002/pip.613.

[88] S. Gonzalez, A. Ellis, M.E. Ropp, C.A. Mouw, D.D. Schutz, S.J. Perlenfein, Unintentional islanding detection performance with mixed DER Types," United States, Tech. Rep. (2018), https://doi.org/10.2172/1463446. SAND2018-8431 666671, https://www.osti.gov/servlets/purl/1463446.

[89] B. Yu, M. Matsui, Y. Jung, G. Yu, Modeling and design of phase shift anti-islanding method using non-detection zone, Solar Energy 81 (11) (2017) 1333–1339, https://doi.org/10.1016/J.SOLENER.2007.06.009.

[90] S. Akhlaghi, H. Meshginkelk, A. Akhlaghi, A.A. Ghadimi, A novel hybrid islanding detection method for inverter-based distributed generation based on frequency

drift, Australian J. Elect. Electron. Eng. 11 (2) (2014) 161–174, https://doi.org/10.7158/E13-085.2014.11.2.
[91] Huili Sun, L.A.C. Lopes, Zhixiang Luo, Analysis and comparison of islanding detection methods using a new load parameter space, in: 30*th Annu. Conf. IEEE Ind. Electron. Soc.,* 2004. *IECON* 2004, Busan, Korea (South) 2, 2004, pp. 1172–1177, https://doi.org/10.1109/IECON.2004.1431741.
[92] H. Vahedi, M. Karrari, G.B. Gharehpetian, Accurate SFS parameter design criterion for inverter-based distributed generation, IEEE Trans. Power Del. 31 (3) (June 2016) 1050–1059, https://doi.org/10.1109/TPWRD.2015.2391193.
[93] E.J. Estébanez, V.M. Moreno, A. Pigazo, M. Liserre, An overview of anti-islanding detection algorithms in photovoltaic systems in case of multiple current-controlled inverters, in: 2009 35*th Annu. Conf. IEEE Ind. Electron.*, Porto, Portugal, 2009, pp. 4555–4560, https://doi.org/10.1109/IECON.2009.5414870.
[94] M.E. Ropp, M. Begovic, A. Rohatgi, G.A. Kern, R.H. Bonn, S. Gonzalez, Determining the relative effectiveness of islanding detection methods using phase criteria and nondetection zones, IEEE Trans. Energy Convers. 15 (3) (Sept. 2000) 290–296, https://doi.org/10.1109/60.875495.
[95] S. Jain, V. Agarwal, Single stage grid connected photovoltaic systems with maximum power point tracking, IEEE Trans. Power Electron. 22 (5) (2007) 1928–1940, https://doi.org/10.1109/TPEL.2007.904202.
[96] X. Zhang, D. Xie, Performance assessment of islanding detection for multi-inverter grid-connected photovoltaic systems, Energy Power Eng. 5 (4) (2013) 1517, https://doi.org/10.4236/EPE.2013.54B287.
[97] A. Lashab, D. Sera, J.M. Guerrero, A dual-discrete model predictive control-based MPPT for PV systems, IEEE Trans. Power Electron. 34 (10) (Oct. 2019) 9686–9697, https://doi.org/10.1109/TPEL.2019.2892809.
[98] H. Abouadane, A. Fakkar, D. Sera, A. Lashab, S. Spataru, T. Kerekes, Multiple-power-sample based P&O MPPT for fast-changing irradiance conditions for a simple implementation, IEEE J. Photovolt. 10 (5) (Sept. 2020) 1481–1488, https://doi.org/10.1109/JPHOTOV.2020.3009781.
[99] B. Yu, An improved frequency measurement method from the digital PLL structure for single-phase grid-connected PV applications, Electronics (Basel) 7 (8) (2018) 150, https://doi.org/10.3390/ELECTRONICS7080150.
[100] Y. Terriche, M.U. Mutarraf, M. Mehrzadi, et al., Adaptive CDSC-based open-loop synchronization technique for dynamic response enhancement of active power filters, IEEE Access 7 (2019) 96743–96752, https://doi.org/10.1109/ACCESS.2019.2929615.
[101] A. Lidozzi, G.L. Calzo, L. Solero, F. Crescimbini, Single-phase inverter for grid-connected and intentional islanding operations in electric utility systems, J. Power Electron. 16 (2) (2016) 704–716, https://doi.org/10.6113/JPE.2016.16.2.704.
[102] S.M. Muyeen, J. Tamura, T. Murata, Stability Augmentation of a Grid-Connected Wind Farm,, Springer Science & Business Media, 2008, https://doi.org/10.1007/978-1-84800-316-3.
[103] A. Lashab, D. Sera, J.M. Guerrero, L. Mathe, A. Bouzid, Discrete model-predictive-control-based maximum power point tracking for PV Systems: overview and evaluation, IEEE Trans. Power Electron. 33 (8) (Aug. 2018) 7273–7287, https://doi.org/10.1109/TPEL.2017.2764321.
[104] A. Lashab, D. Sera, F. Hahn, et al., Cascaded multilevel PV inverter with improved harmonic performance during power imbalance between power cells, IEEE Trans. Ind. Appl. 56 (3) (May-June 2020) 2788–2798, https://doi.org/10.1109/TIA.2020.2978164.
[105] E. Ropp, M. Begovic, A. Rohatgi, Prevention of islanding in grid-connected photovoltaic systems, Progress in Photovoltaics: Res. Appl. 7 (1) (1999) 39–59, https://doi.org/10.1002/(SICI)1099-159X(199901/02)7:1≤39::AID-PIP246≥3.0.CO;2-J.
[106] Standard conformance test procedures for equipment interconnecting distributed energy resources with electric power systems and associated interfaces, IEEE 1547 (2020) 1–2020, https://doi.org/10.1109/IEEESTD.2020.9097534.